Journal Home Page: https://sites.google.com/a/univsul.edu.iq/sjes

Review Article:

Integration of solar panels with the architectural context of residential buildings, Erbil city as a case study

Binyad Maruf Abdulkadir[1]
Polla Dilshad Ibrahim[1]

[1]Salahaddin University - Eebil, College of Engineering, Department of Architecture

Article Inform

Article History:
Received 9 June 2019
Accepted 16 April 2020
Available online 1 June 2020

Keywords: Photovoltaics, Residential Buildings, Architectural Integration of PV, BIPV, PV, Renewable Energy, Iraqi Kurdistan Region.

About the Authors:
Corresponding author:
Polla Dilshad Ibrahim Sktani - MSc.
E-mail: polla.ibrahim@su.edu.krd
Researcher Involved:
Binyad Maruf Abdulkadir Khaznadar - MSc.

DOI Link: https://doi.org/10.17656/sjes.10125

Abstract

In the last few decades, sustainable buildings and incorporating renewable energy become crucial to preserve life for current and next generations. Photovoltaics (PV) are widely used to produce energy for buildings which it can be seen worldwide and in Iraqi Kurdistan too. However, their integration into buildings, including residential buildings, become problematic for architectural quality of the buildings in general and residential buildings specifically as it is not integrated well and most of the times seem as it is not belong to it because they were not designed in congruence with the architectural form. Based on this, the researchers explored different innovative architectural integration approaches in developed world and innovative products that enable them to architecturally integrate it that can improve architectural quality besides generating solar energy in Iraqi Kurdistan. PV products have been divided for roofs and façades (with all it is parts) so that it can architecturally integrate better. An analysis for the rate and quality of used PV in Kurdistan has been done through set of criteria's so that to specifically determine the problems, and through the analysis creating a residential (house) prototype and applying potential BIPV on it. Recommendations have been presented for how it can be architecturally integrated besides it is energy production.

1. Introduction

In the time when the discourse of climate change issues is prevalent in the world which is basically due to excessive use of fossil fuel, the use of various types of solar energy is relevant and crucial. This use of renewable energy sources like solar panels is much needed in developing countries like Iraqi Kurdistan as there is huge shortage of electricity too. That is why the use of solar panels becoming more and more popular and it can be seen in many houses and other

types of buildings in the region (as shown in Figure 1, and other 9 examples in the appendix) despite it is not being financed and promoted by the government.

2. Problem Statement

It is evident that the use of solar energy for energy production is clean and renewable method that requires minimum maintenance. However, their integration into buildings; including residential buildings, represents a real architectural challenge, as to a great degree, the development of solar systems for energy has been characterized by the wish for energy effectiveness, while the architectural aspects have been neglected in the Iraqi Kurdistan Region. Therefore, there is a lack of knowledge between PV and their integration to the buildings in the region.

There are some problems when these solar photovoltaics implemented on residential buildings due to lack of good architectural quality as it is not meeting desired design considerations. As it can be seen in figure 1 and other examples in appendix, the panels do not look like they belong to it because they were not designed in congruence with the architectural form. It is important to note that solar facilities should not be regarded as technological systems that only serve the purpose of producing electricity; instead, they must be regarded as elements that make an important contribution to the architectural design. Innovative approaches have to be explored in terms of design and implementation in order to match the modern technological components in terms of proportion, material, colour and balance of residential buildings.

3. Research Aim

The aim of this research is to explore possible ways of integrating PV technologies into residential buildings (houses), in order to add emphasis on the overall architectural expression in addition to its energy production role. It will focus on design possibilities regarding the use of solar technologies into buildings with some innovative approaches, basic focus is on the aesthetics part of integration as this makes the major effect on the people and the building. PVs can deliberately be used as architectural design elements and improve integrity.

4. Research Question

How can the solar panels (Photovoltaic, PV) be architecturally integrated into buildings, specifically residential buildings, to serve purpose of enhancing architectural quality besides generating solar energy in Iraqi Kurdistan Region?

5. Research Hypothesis

PV can be architecturally integrated to the buildings to add value to the aesthetics of the building, including residential buildings; and it can be used as building element.

6. Research Methodology

The researchers studied architecturally integrated PV examples of international case studies through the literature in the theoretical framework, so that to derive set of factors that affects integrity of PV panels with architectural form, and also studied criteria's of what makes a good architectural PV integration. On the other direction, the researchers analysed local PV house examples in Erbil, derived findings. Then created a prototype based on these findings, after that the potential successful PV integration in which gained from international examples is applied to the local prototypes.

7. What Is Photovoltaic (PV)

PV's are usually based on silicon and are used to convert solar radiation into electricity. Direct current (DC) is generated when the devices are exposed to either sunlight or daylight, as PVs respond to both direct and diffused radiation. The electricity generated is either used directly into DC appliances or converted to AC using inverters. It can also store the energy using batteries to be used during night. On the other hand, Photovoltaic cells are sustainable, quiet, and require minimal maintenance. In a PV system, cells combine to form modules, which give the system the flexibility to be expanded or reduced to suit any given application for their integration into new and existing buildings. Although the most commonly used cell types come from the same base material silicon, different technologies offer cells with different technical and aesthetic characteristics (Basnet, 2012).

Common PVs available are mono-crystalline silicon, polycrystalline silicon and thin film silicon called amorphous silicon (A-Si) (Thomas et al., 2001). However, many new types have been developed recently in pursuit of high technology advancement and better integration with buildings.

8. Types of Photovoltaic Installation

Typically, there are two types of PV installation, which are:

A- BAPV

Building Applied Photovoltaics (BAPV) is the installation of conventional photovoltaic cells on building roofs, with almost standard sizes and shapes. This adds an extra load to the roof members (Ogunkeye, O., 2017). This type is common in Kurdistan Region.

B- BIPV

Building Integrated Photovoltaics (BIPV) can act as multifunctional solar products that generate electricity through photovoltaics while serving as construction materials and building elements, as shown in figure 2. (Ogunkeye, 2017).

- BIPV can be parts of a building's envelope, like roof cover, wall facing and glazed surfaces.
- They can be solar protection devices like sun shadings, additional architectural elements such as canopies, balcony parapets, and any other architectural element of a building.
- Nowadays BIPV products come in different sizes, shapes, colours and functions. They are highly flexible in terms of size and attractive as the defining element in a building's design. (Simon and Guriento, 2009).

In principle, BIPV can be used in all parts of the building envelope. Although roof surfaces are the preferred area for installing PV elements due to their advantageous irradiation values, façades also offer enormous potential (Ogunkeye, 2017).

9. Integration of Photovoltaics

In case the PV becomes part of the residential building skin, it gains multiple functions and requires aesthetical integration into the overall design concept (Farkas, 2011). Both roofs and facades can be explored for the architectural potential of integration. Any part of the roof or external walls that is exposed to sunlight or daylight e.g. skylights, claddings, windows, external shading devices and railings can be used for PV integration.

Integration of PV into buildings has the following advantages (Reijenga et al., 2011):

- In cities with high density where the value of land is high, installing PV on part of buildings is beneficial.

- PV wall or roof replace the construction material, and hence replaces its cost.
- Power is generated on site and replaces electricity that would otherwise be purchased and avoids distribution losses.
- Architecturally elegant, well-integrated systems will increase market acceptance.
- Building-integrated PV (BIPV) systems provide building owners with their environmental commitment to public.

9.1. Roof Integration of PV

A PV system can be integrated into the roof in several ways. One choice is for the integrated system to be part of the external skin. There are also many products for small-scale use to suit the scale of the roof covering, for example, PV shingles and tiles. The small scale of these products makes them very convenient for use in existing buildings. Transparent PV modules used as roofing materials serve as water and sun barriers and also transmit daylight (Reijenga and Kaan, 2011).

9.1.1. PV in flat roof

PVs laid horizontally on the flat roofs are normally not visible from the ground from efficiency view point, mono and poly-crystalline PV systems produce the most energy when their angle is optimized to that of the sun. Unlike to this, thin films work equally well even when laid horizontally on flat surfaces proving to be the best options for integrating into flat roofs. Some PV examples developed by Lumeta PowerPly can be integrated on flat roof, which is a part of a fully integrated roofing system. Others can be integrated as Saw tooth roof like the DIY store, Hamburg as shown in figure 3.

9.1.2. PVs on Inclined/ Pitched roof

Architectural aesthetics should be taken into consideration while integrating as these are visible parts of the building. Usually the aesthetics is lost if the color of the roofing material is different from that of the PV (Basnet, 2012). Examples can be found in figure 4.

9.1.3. PV tiles or shingles

The advantage of PV tiles or shingles over panels is that they look similar to roofing tiles, are available in different colors and are aesthetically more pleasing, having features of a good architectural integration, as shown in figure 5.

9.1.4. PVs in Atrium/skylights

PVs can equally be integrated as multifunctional elements in transparent roof structures or atriums that allow controlled light into the interior. As semi-transparent roof units, they can protect the building from heat, sunlight, and glare. Well-designed PV integrated atriums may also be a strong feature of the building when viewed from the interior. In glass-covered areas, such as atriums, sun protection on the roof is necessary in order to avoid overheating in summer. The PV cells absorb 70-80% of the sun radiation (Reijenga and Kaan, 2011).
There are many possibilities available, as each layer of the module from the front glass surface to the reverse side of the glass can be textured and coloured, as shown in figure 6.

9.2.. Facade integration of PV

It is a normal building practice that external walls of buildings are covered with insulation and protective cladding. This cladding can be wood, metal sheets, panels, glass or PV modules. On the other hand, Transparent and semi-transparent

modules of PV have been developed that are used in curtain walls for controlling daylight in addition to producing energy. The semi-transparent glazing prevents direct sunlight from entering the building, which reduces cooling loads and glare (SHC, 2012).

9.2.1. Opaque façade

PV can be integrated into the opaque parts of the façade, it can be integrated as cladding on to solid parts of façade, as shown in figure 7. The sizes are flexible and custom made according to each project.

9.2.2. Translucent façade

PV can be integrated into it glazed parts of façade as semi-transparent and translucent façade, as shown in figure 8. Usually the height is according to window height, as it is custom made.

9.2.3. Shadings

Photovoltaic modules can be used as shadings, like overhanging PV shade screens or blinds over a window, as shown in figure 9 and 10.

10. Architectural Integration: Criteria For Goode PV Architecture.

As aesthetics is subjective, therefore some agreed criteria should be established for determining what is regarded as good PV integration in architectural means. Upon that, the IEA PVPS program defined a specific task entitled "Photovoltaics in the Built Environment (Task 7)". According to Kaan, & Reijenga, (2004), ten team member experts cooperated on this project from the various countries which all of them have an architectural background. "The team studied which key requirements needed to be complied with (design criteria for good-quality PV projects) in order to produce successful PV integration. A small group of experts formulated a number of (not too subjective) criteria whereby integration of PV in buildings could be architecturally classified and evaluated. The criteria can be used as a guideline for both the designer and the architectural critic" (Kaan & Reijenga, 2004).

50 BIPV projects evaluated in written form by each of experts individually and anonymously. Each wrote their notes, and then similar notes collected, classified and combined to form agreed criteria. After that, the projects evaluated based on these defined criteria's.

According to (Kaan, & Reijenga, 2004), the following aesthetic criteria were finally accepted as being vital to a successful BIPV project.

1. Natural integration,
2. Designs that are architecturally pleasing,
3. Good composition of colors and materials,
4. Dimensions that fit the grid of building, harmony, composition,
5. PV systems that match the context of the building,
6. Well-engineered design,
7. Use of innovative design.

10.1. Natural integration of the PV system

This means that the PV system seems to form a logical part of the structure and adds the finishing touch to the building. The PV system does not have to be that obvious. In renovation situations the result should look as though the PV system was there before the building was renovated. As shown in figure 11.

10.2. The PV system is architecturally pleasing, within the context of the building

The design must be architecturally pleasing. The building should look attractive and the PV system

adds attention-grabbing features to the architecture. This is a very subjective issue, but there is no doubt that some buildings are considered more pleasing than others. As shown in figure 12.

10.3. Good composition of colors and materials

The color and texture of the PV system is in harmony with the other materials, as shown in figure 13.

10.4. The PV system fits the grid, or visual pattern of the grid (is in harmony with the building and, as a whole, forms a good composition)

The dimensions of the PV system should match the dimensions of the building. This will determine the dimensions of the modules and the building grid lines used, As shown in figure 14.

10.5. The PV system matches the context of the building (contextually)

The appearance of the building, as a whole, should be consistent with the PV system used.
In a historic building, a tile-type system will look better than large modules, if the PV system cannot be placed out of sight. A high-tech PV system, however, would look better on a high-tech building. As shown in figure 15.

10.6. The system, and its integration, are well engineered

The elegance of design details is taken into account. All details are well conceived, the amount of materials is minimized, as shown in figure 16.

10.7. The application of PV has led to innovative designs

PV systems have been used in many ways, but there are still countless new ways to be developed. This is all the more reason to consider this criterion, in addition to the other considerations, as shown in figure 17.
Gaiddon et al, (2009) point out that "as buildings, and consequently building-integrated PV, form a part of the perception of urban aesthetics, the above criteria may also be applied when it comes to giving a value judgment of the urban environment."

11. Website for "Innovative solar products for architectural integration".

According to an international web survey conducted by (IEA Task 41.A.1) in 2012, the major barrier for lack of use of PV and other renewable products were low architects knowledge and low products inerrability. Based on this, they designed a website to address these issues by providing both the innovative solar products available on the market today and, on the other hand, the information needed to optimally integrate them in the building in general, as shown in figure 18. The website designed to be ergonomic and attractive to architects and their clients, (Probst et al, 2014).
By choosing a specific technology and an integration type (roof, façade, ..) the user gets access to a selection of appropriate products, presented in the form of A4 sheets. These sheets include architect oriented information, contact details and pictures, both on the product alone and situation examples in buildings. The website is completed by a set of documents.

12. Practical Study Of Research

The researchers analyzed local PV examples in Erbil, derived findings regarding use, rate and quality of local applied PV buildings which is enhanced by statistical tools and bar charts, detecting problems regarding architectural quality. Then created a prototype based on these findings, after that the potential successful PV integration in which gained from international examples is applied to the local prototypes. The potential PV integration applied to prototype shows that how successfully integrated PV can be applied on the prototype houses in Erbil to serve purpose of enhancing architectural quality.

a) Analysis of existing used PV in Erbil, Iraqi Kurdistan.

After exploring the above literature on architectural integration of PV on buildings worldwide, the researchers of this study analyzed 10 random samples of existing buildings (majority are houses) that used PV in Erbil, Iraqi Kurdistan. Several criteria have been established to examine the rate and quality of photovoltaics used on these houses, and to determine specific problems of PV's used, as explained in table 1.

As it can been seen from the table, all the used PV has been put on the roofs, and all are applied or mounted to roof with BAPV installation system. This system usually does not integrate well with the aesthetics and building form.

Regarding other factors, majority of examples have negative effect on: overall building form, color, material, and proportion & balance. As shown in figure 19.

Out of 10 examples that used PV on their buildings in Erbil, it is found out that 90% are residential row houses, while only 10% of examples are commercial building, as shown in figure 20. This is shows that the PV is more demanded for residential sector rather than other sectors. It seems that houses suffer the most due to electricity shortage and that is why they tend to produce electricity using mounted PV in the roofs, therefore the researcher focused on houses as a prototype in practical study.

Regarding number of floors of the houses which used PV, 89% of houses are two floors, whilst only 11% of houses are one floor. As shown in figure 21.

Regarding type of the roofs, most of the houses have a flat roof 89%. About 11% have an inclined roof, as inclined roof is not common in Erbil. On that 89% of flat roof type, some of them have a few simply inclined features on the façade like inclined red tiling for decoration (qrmeed). See figure 22

Regarding presence of balconies and it is numbers, about 37.5% of the houses have one balcony, same percentage with two balconies. While only 12.5% have either three balconies or no balcony at all. As shown in figure 23.

Regarding the outline of houses, most of the houses under 250 m2 have a recessed plan to make a room for the parking, also to provide a shade against harsh weather conditions like rain or excessive heat in summer. However, some houses larger than 300 m2 may have a straight façade, As shown in figure 24.

On the other hand, the analysis focused on the void to solids, specifically void percentage in the facades of the houses in Erbil. By voids the researchers mean all windows and doors in the façade. The graph shows the percentage of voids in the examples. It is between 20% to 42%, the mean is 32.1%, which means almost one third of the houses façade are openings-voids (windows and doors). As shown in figure 25.

b) Finding a prototype

Based on above analysis, the following prototype has been established as shown in table 2. According to findings from analysis, it shows

that people apply PV on the residential sector especially row houses. It is two floor house having a flat roof based on the analysis above, having 32% opening in the façade, with the possibility of having one to two balconies. All the findings of the analysis have been applied to prototype.

c) Applying architecturally integrated PV (BIPV) on the created prototype

After creating a prototype house that represent common houses of Erbil, the researchers created visually enhanced image based PV integration, the architectural PV integration represent potential design of BIPV on the prototype as shown in table 2.

"The aesthetics of an urban area are largely determined by the architectural quality of the buildings; both the individual buildings and the aesthetic relations between the various buildings" (Gaiddon et al, 2009). Therefore, by improving architectural quality of single buildings, the context will be harmonized and improved too. In other words, as described in criteria of good PV architecture integration, contextuality means the total image of a house or building is in harmony with the PV system.

d) Shapes, dimensions, and other details of solar panels for both existing examples and proposed prototype

From the building integration point of view, the market is divided into two main categories: the standard modules, which is Building Applied Photovoltaics (BAPV) type as discussed in literature, and the building dedicated products or customized, which is Building Integrated Photovoltaics (BIPV) products that offer enormous flexibility in terms of shape, size, dimensions, texture and color (Probst & Roecker, 2011).

All examples of PV used in Erbil city have used BAPV type. The researchers of this study visited several local PV providers and the mentioned PV samples in Erbil. It has been found that the PV which is available in market for residential use are in two standardized sizes, first one is 196cm*99cm (Rectangle shape), and other type is 163cm*98cm (Rectangle shape), as shown in table 3. It can be applied on roofs either in portrait or landscape orientation. The most common color is blue; while there is few samples have black color too. Their fixed sizes and explicit frames can be problematic for architectural integration of projects including houses.

Regarding electricity production, many factors effect on PV efficiency like climate, loss of energy during transmutation, battery and invertor types, location, daily temperature…etc. According to local PV providers and visited case study householders in Erbil, a single 196cm*99cm panel of PV which equals 1.94 m^2 of PV gives around 1.25 to ~ 1.0 ampere (amp) of electricity, excluding all loses. That's why it can been seen from table 3 that existing PV case study houses in Erbil have at least four panels of 196cm*99cm in dimension which equals to around 4 amp of electricity, as this is a minimum energy any house gets from local district generators. This data will be used to determine necessary area needed for PV to be applied on house prototype, as shown in figure 36, because the area of prototype is much more than any existing samples for applying PV and generating energy, as shown in figure 36.

However, BIPV products are quite flexible in terms of shape, size, color, texture…etc. It can be customized according to architects desire and needs, offers the possibility of custom-made products individually produced for a certain project (Probst & Roecker, 2011). Regarding size, it can ranges from 0.2 m^2 to 2 m^2, with availability of 10cm*10cm cells and 12.5*12.5cm and so on as it will be custom made. Regarding color, it can

be brown, blue or black, reddish brown, chocolate brown, hepatic and sage green colors. Regarding transparent PV modules, most of them available in frameless option as a way to enhance appearance.

To achieve quality in the architectural integration of PV system, certain points had been applied to prototype and achieved. These are: multi-functionality of PV, shape and size, color, material and surface texture, flexibility in integration and types of jointing, as shown in table

13. Conclusions

The work shows that the architectural integration of PV systems is possible. It adds values and the aesthetical characteristics for the buildings. The BIPV systems have great flexibility with enormous ways to integrate with the roof, façade or any other elements of any building.

The guidelines or criteria for the good architectural integration for achieve good quality and homogeneity has been described and explored. An easy navigated website for PV products has been shown which can help architects to better understand and integrate PV to their designs. Based on that, now it is clear how to do architectural integration in terms of size and position, color, surface texture, materials and harmony with overall composition in Iraqi Kurdistan.

These BIPV integrations will be multifunctional, as it acts as building element besides it is PV role which is energy generating. The research shows that PVs can be used as architectural design elements in a distinctive way.

Finally, as explained above, solar facilities should not be regarded as technological systems that only serve the purpose of producing electricity; instead, they must be regarded and treated as elements that make an important contribution to the architectural design.

14. Recommendation

- Architectural integration of PV using BIPV is important; the well-designed integration adds value to the aesthetics of the building. Therefore it should be used as opposed to the current BAPV installation type.
- PV is quite flexible, many technological advances are developed for PV to meet desired pattern and design in order to meet architectural criteria's mentioned in Section 10.
- Using mentioned criteria, and exploring website about PV products and it is possible architectural integration will increase the PV use by architects in their designs and as a result better PV integration will be possible.
- Local municipalities and other related authorities should legalize architectural integration of PV in order to form a part of building aesthetics. As in many countries local authorities set architectural and visual conditions relating to the appearance of new or renovated buildings.
- Using PV panels preferred to be developed during design stage, in order to be part of the design.

References

1- Basnet A., (2012), Architectural Integration of Photovoltaic and Solar Thermal Collector Systems into buildings.
2- Farkas K., Horvat M. et al. (2012), Building Integration of Solar Thermal and Photovoltaics. Barriers, Needs and Strategies, IEA SHC Task 41 Solar energy and architecture.
3- Farkas, K. (2011), Facade Integration Typologies of Photovoltaics.

تكامل الالواح الشمسية مع السياق المعماري للابنيه السكنية مدينة اربيل كنموذج للدراسه

بنياد معروف عبدالقادر [1] - ماجستير
پۆلا دلشاد ابراهيم [1] - ماجستير
[1] جامعة صلاح الدين - اربيل ، كلية الهندسة ، قسم العمارة

المستخلص

في العقود الاخيرة اصبحت الابنية المستدامة وادارة الطاقة المتجددة من المواضيع الهامة التي تم التطرق اليها في شتى الميادين ، وذلك لفرض انقاذ هذا الكوكب و وفير حياة هانئة للاجيال اللآتية. اصبح استخدام (الالواح الشمسية) في المباني رائجا وبشكل واسع كوسيلة لانتاج الطاقة في العالم وكذلك في اقليم كوردستان العراق. اصبح استخدام (الالواح الشمسية) يشكل عائقا في العملية التصميمية للمبنى في كثير من الاحيان ،بما في ذلك المباني السكنية ، خاصة عندما لا يتم تكاملها مع الشكل المعماري. على هذا الاساس قام البحث بدراسة الوسائل الحديثة في استخدام (الالواح الشمسية) بشكل متكامل مع الشكل المعماري ، وكذلك دراسة الاشكال الحديثة للالواح الشمسية وهي عبارة عن عناصر معمارية يتم استخدامها في الابنية بشكل العام والابنية السكنية على وجه الخصوص ، والتي يتم انتاجها من قبل شركات مختصة متماشيا مع التصميم المعماري ، و بذلك يتم الاستفادة من هذه الالواح كوسائل لتوليد الطاقة النظيفة وكذلك اضفاء قيمة جمالية للمبنى السكني. وكذلك قام البحث بدراسة هذه التطبيقات في اقليم كوردستان العراق. بشكل عام يتم استخدام الالواح الشمسية في السطوح وكذلك في واجهات المباني من خلال عناصر الواجهات واجزائها ، وبذلك يتم استخدام هذه الالواح بشكل متكامل مع اجزاء المبنى و بشكل افضل. قام البحث بدراسة المعايير لاستخدام الالواح الشمسية في اقليم كوردستان وفي مدينة اربيل على وجه الخصوص. وكذلك قام البحث بتشخيص المشاكل في استخدام هذه الالواح من خلال عينات دراسية تم اختيارها، ومن خلال عملية التحليل تم التوصل الى نمط للوحدة السكنيه من اجل تطبيق نظام "الالواح الشمسية بشكل متكامل مع الشكل المعماري" عليه. قام البحث بكتابة توصيات لاستخدام الالواح الشمسية بشكل تكاملي وذلك لفرض توليد الطاقة واخذ الجانب الجمالي بنظر الاعتبار.

الكلمات المفتاحية : الالواح الشمسية ، الأبنيه السكنية ، التكامل المعماري مع PV (PV, BIPV) ، الطاقة المتجددة ، اقليم كوردستان العراق.

4- Farkas, K., et al (2009), Architectural Integration of Photovoltaic Cells, Overview of materials and products from an architectural point of view,SASBE 2009, The Hague, The Netherlands.
5- Gaiddon, B, Kaan, H and Munro, D (eds) (2009), Photovoltaics in the Urban Environment: Lessons Learnt from Large-Scale Projects, London: Routledge, https://doi.org/10.4324/9781849770149. [Accessed 5 January, 2020].
6- IEA Task 41 database on innovative solar products for building integration, https://solarintegrationsolutions.org/. [Accessed 24 September, 2019].
7- Kaan, H. & Reijenga, T. (2004). Photovoltaics in an Architectural Context.
8- Ogunkeye, O. (2017), The advent of Building Integrated Photovoltaic– BIPV and Building Applied Photovoltaic- (BAPV) as standalone off grid clean energy source in Nigeria.
9- Probst, M. Deschamps, L. & Roecker, C. (2014). Innovative solar products for architectural integration: a joint IEA tasks 41 and 51 website. EPFL, Switzerland.
10- Probst, M. C. M., & Roecker, C. (2011). Architectural integration and design of solar thermal systems. Lausanne. EPFL Press.
11- Reijenga T, (2000) ,"Photovoltaic Building Integration Concepts – What do Architects need?" Proc. IEA PVPS Task7 Workshop Lausanne Featuring A Review of PV Products, IEA PVPS Task7, Halcrow Gilbert, Swindon.
12- Reijenga, T. H. & Kaan, H. F. (2011). PV in Architecture. Handbook of Photovoltaic Science and Engineering. Second ed.: John Wiley & Sons.
13- SHC. (2012). IEA SHC Task 41 Solar Energy and Architecture [Online]. Available: http://task41.iea-shc.org/ [Accessed 19 September, 2019].
14- Simon R. and Guriento N., (2009). Building Integrated Photovoltaics/a handbook, Birkhäuser, Basel, Switzerland.
15- Thomas, R., Fordham, M. & Partners (eds.) 2001. Photovoltaics and Architecture, London: Spon Press.

Fig.1: (Example 1) House in Ronaki Qr., Erbil. The panels do not look like they belong to building because they were not designed in congruence with the architectural form. (Source: Researcher)

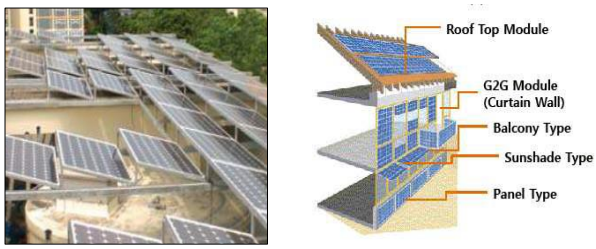

Fig.2: (Left) BAPV system for installation, (Right) BIPV for various applications. (Source: Ogunkeye,2017)

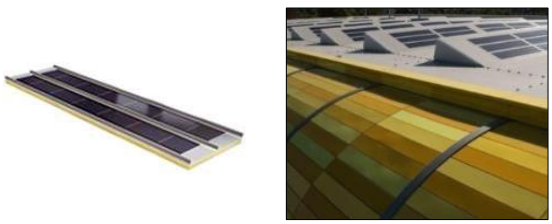

Fig.3: (left) Developed by Lumeta PowerPly, it can be integrated on flat roof, is a part of a fully integrated roofing system (right), Sawtooth roof with PV integration, DIY, Hamburg, Germany.
(Source: Basnet 2012)

Fig.4: (Left) Integrated PV on the pitched roof of vacation house Bartholomä-Park in Germany (middle & Right) Integrated PV roofs in Schlierberg Solar Settlement housing estate in Freiburg, Germany. (Source: Basnet 2012)

Fig.5: (left) Roof with integrated PV tiles, (right) PV shingles. (Source: Basnet 2012)

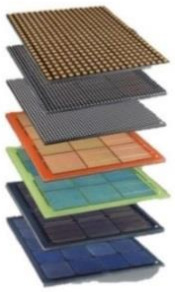

Fig.6: (Left) PV samples for skylight in different colors & textures, (middle & right) Atrium with PV modules, Ludesch/Vlbg., Austria. (Source: ttps://solarintegrationsolutions.org)

Fig.7: (left) bronze and gold colored PV cells used in the "home+" building project, tuttgart, Germany, (right) PV integrated into the opaque parts of house in Seoul, South Korea. (Source: Basnet, 2012)

Fig.8: (left) frameless, translucent PV installed in residence home in Calgary, Canada (right) PV integrated into it south glazed façade in Tobias Grau production building in Germany. (Source: https://www.skyfireenergy.com)

Fig.9: (left, middle) Integration of PV on the sliding sun shading, dwelling houses in Spinnereistraße, Austria, (right) PV used as shading in the Energy Research Centre, Netherlands. (Source: Basnet, 2012)

Fig.10: Solar PV blinds over a window. (Source: https://inhabitat.com)

Fig.11: (left) J-House, Tokyo, Japan. Natural integration of the PV system in the building. Architect: Jiro Ohno, (right) The dwellings at the 5 MW project in the HAL district, Langedijk, Netherlands. It has a large PV roof without any perforations. This strengthens the architectural expression of the roof design. Source: (Gaiddon et al, 2009)

Fig.12: (left) PV shadings as sun protection in the façade, these vertical blinds makes it visually attractive. Design: ABZ Architects, Netherlands. (Kaan, & Reijenga, 2004). (Right) 'Plus-Energie' house, Weiz, Austria. PV used in curved façade adds to the image of the building. Architect: Erwin Kaltenegger, Austria. (Source: Gaiddon et al, 2009)

Fig.13: (left) Color and texture harmonize together in this historical building, horse stables in Bern, Switzerland. (Right) The facade consists of three blocks of colour, so that the block with blue solar panels harmonizes with the adjacent brick-colored blocks. Apartments in the Netherlands.
(Source: Kaan, & Reijenga, 2004).

Fig.14: (left) surplushome, a PV cladded house in Darmstadt, Germany, (Right) 'Solar Cube' at the Discovery Science Museum in Santa Anna, Los Angeles, USA. (Source: Probst & Roecker, 2014)

Fig.15: (left) This type of PV system blends well with the traditional Japanese slate-type roof. Houoh, Japan. (Right) color of roof cladded PV is in harmony with the context of house and surrounding colors and grids. (Source: Probst & Roecker, 2014)

Fig.16: Single Family House, Gutenberg, Austria, solar cells are protected by a coat of safety glass, the modules are attached to the balustrade and works as a balcony railing protector. (Source: Probst & Roecker 2014)

Fig.17: Single-family houses 'De Keen', Etten-Leur, The Netherlands. The application of PV has led to a new architectural concept. Architect T. H. Reijenga, BEAR Architekten. (Source: Gaiddon et al, 2009)

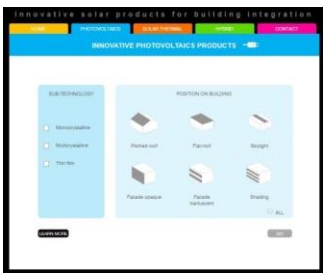

Fig.18: Innovative solar products for architectural integration website: (Source: https://solarintegrationsolutions.org)

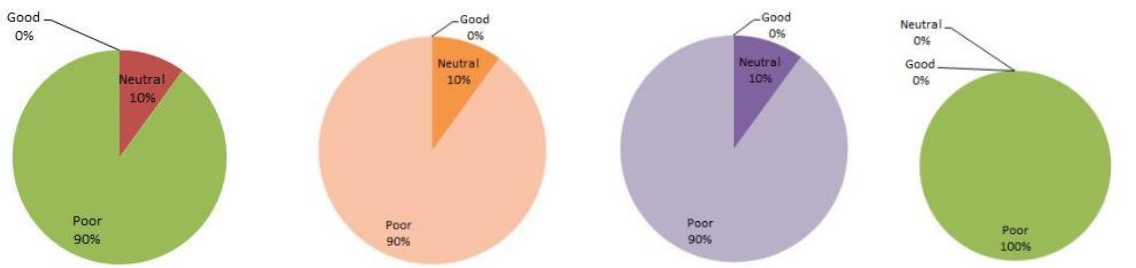

Effect of visible PV on overall architectural quality.

Proportion &balance with the building.

Colour match with overall form.

Material & surface texture.

Fig.19: analysis of ten examples that have negative effect on: overall building. form, color, material, and proportion & balance. (Source: Researcher)

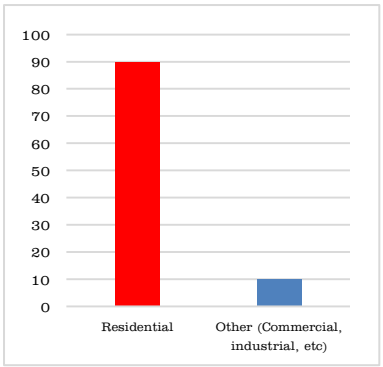

Fig.20: Existing Used PV according to building sector. (Source: Researcher)

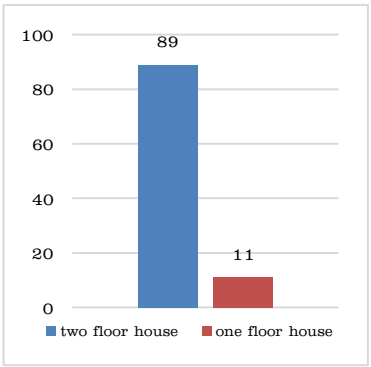

Fig.21: number of floors of the houses. (Source: Researcher)

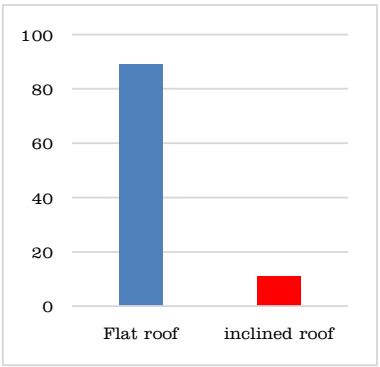

Fig.22: Type of roofs. (Source: Researcher)

Fig.23: Presence and number of balconies. (Source: Researcher)

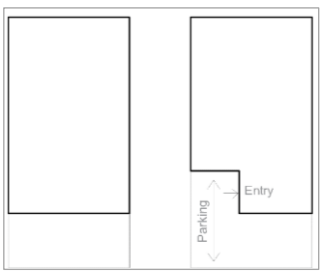

Fig.24: outline of the houses in the top view. (Source: Researcher)

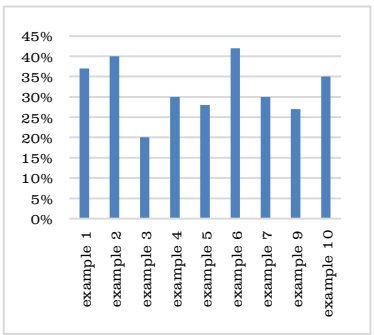

Fig.25: void percentage in the facades of the houses in Erbil. (Source: Researcher)

Fig.26: (Example 2) House in Sarbasty, Erbil, Iraqi Kurdistan. As it can be seen, the PV is visible as an added element on the building. It produces an architectural result that appears as "un-designed". (Source: Researcher)

Fig.27: It is effect on context is much noticeable at some distance from the house. (Source: Researcher)


Fig.28: (Example 3) Korean Village, Erbil. The color of PV is not matched with the roof colour. (Source: Researcher)


Fig.29: (Example 4) New Zanko Village Qr, Erbil. (Source: Researcher)


Fig.30: (Example 5) Zaytoon city, Erbil. (Source: Researcher)


Fig.31: (Example 6) house in dream city, Erbil. (Source: Researcher)



Fig. 32: (Example 7) House in 184 Qr, Naznaz, Erbil. (Source: Researcher)

Fig.33: (Example 8-a) (right) Ishtar sweets building, Erbil. Undesirable, added on PV visible on the roof of the building. (Example 8-b- alternative) (left) house with undesirable PV structure in dream city-Erbil. (Source: Researcher)

Fig.34: (Example 9) house in Ronaki Qr. Erbil. (Source: Researcher)

Fig.35: (Example 10) house in Dream city, Erbil.
(Source: Researcher)

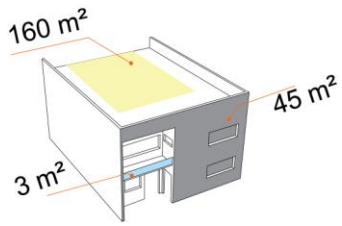

Fig.36: Available areas of prototype so that PV can be applied on it for creating required electricity; it shows it has much more area than any of existing examples.
(Source: Researcher)

Table 1: Analysis of existing used PV on buildings in Erbil. (Source: Researcher)

		Example 1	Ex. 2	Ex. 3	Ex. 4	Ex 5	Ex. 6	Ex. 7	Ex. 8	Ex. 9	Ex. 10
Location of PV	Roof	✓	✓	✓	✓	✓	✓	✓	✓	✓	✓
	Façade										
	Existing land around building										
Type of installation	BAPV	✓	✓	✓	✓	✓	✓	✓	✓	✓	✓
	BIPV										
Visibility level	From distance	✓	✓	✓	✓	✓	✓	✓	✓	✓	✓
	Near the building	✓	✓	✓	✓	✓	✓	✓	✓	✓	

		Example 1	Ex. 2	Ex. 3	Ex .4	Ex. 5	Ex. 6	Ex. 7	Ex. 8	Ex. 9	Ex. 10
Effect of visible PV on overall architectural quality	Good										
	Neutral			✓							
	Poor	✓	✓		✓	✓	✓	✓	✓	✓	✓
Color match with overall form	Good										
	Neutral		✓								
	Poor	✓		✓	✓	✓	✓	✓	✓	✓	✓
Material & surface texture	Good										
	Neutral										
	Poor	✓	✓	✓	✓	✓	✓	✓	✓	✓	✓
Proportion & balance with the building	Good										
	Neutral			✓							
	Poor	✓	✓		✓	✓	✓	✓	✓	✓	✓

Table 2: Applying BIPV on the prototype. (Source: Researcher)

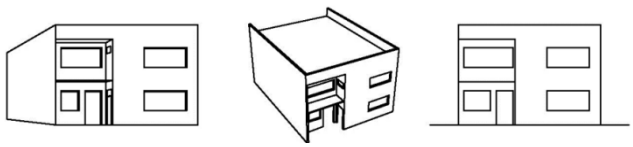

Typical prototype

Integration of PV	location of PV	Proposed PV integration on prototype in Erbil	Dimensions*	Notes
Roof integration	Flat roof 	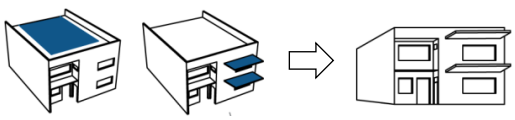	Any grid is possible, as small as 10cm * 10cm to 60cm*80cm , or 1m * 2m as largest.	PV installed directly on the roof regardless of orientation, and it will cover the roof as a construction material.
	Inclined roof 		Usually shingle tiles dimension or red tiles, 10cm * 10cm or more	Inclined roof is not common in Erbil as a type of roofs, only few inclined features can be used.
	Atrium/ skylights 		Can be custom made acc. to skylight/ atrium width. 1m*1m, or 60cm*80cm etc	Can be used as both skylight and PV, usually transparent/ semi-transparent
Façade integration	Opaque façade 	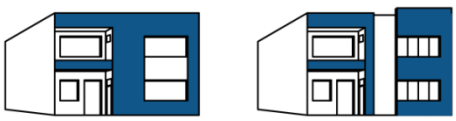	Any grid is possible, as small as 10cm * 10cm to 1m *2m	PV works as cladding on the façade. Various design potentials is possible.
	Translucent façade 	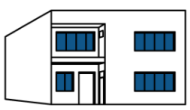	Can be custom made according to window height, which is usually 1.20 m or 1.40m	Semi-transparent glass can work as glass and PV at the same time.
	Shadings 	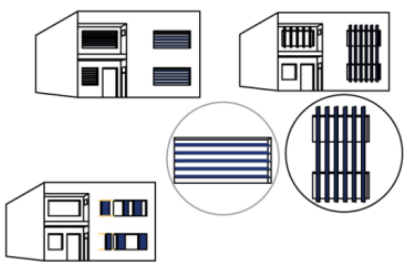	Horizontal shadings can range from 10 cm to 80 cm * window length. Vertical shadings from 10 cm to 80 cm is preferred * window or facade height	PV can be used as both horizontal shading and vertical shadings. It can be used as sliding (movable) shutters too.

Dimensions*: As it is custom made and flexible using BIPV system, dimension can be varied.

Table 3: PV details of existing local examples in Erbil. (Source: Researcher)

Local examples in Erbil	Dimension of single panel (BAPV)	Number of solar panels	Area of all solar panels	Shape and orientation	Potential electricity output
Example 1	163cm * 98cm	57	91 m²	Rectangle 	≃ 47.3 amp
Example 2	196 cm* 99cm	24	46.5 m²	Rectangle 	≃ 23.9 amp
Example 3	196 cm* 99cm	4	7.76 m²	Rectangle 	≃ 4 amp
Example 4	196 cm* 99cm	18	34.9 m²	Rectangle 	≃ 17.9 amp
Example 5	196 cm* 99cm	12	23.2 m²	Rectangle 	≃ 12 amp
Example 6	196 cm* 99cm	24	46.5 m²	Rectangle 	≃ 23.9 amp
Example 7	196 cm* 99cm	8	15.5 m²	Rectangle 	≃ 8 amp
Example 8	196 cm* 99cm	18	34.9 m²	Rectangle 	≃ 17.9 amp
Example 9	196 cm* 99cm	12	23.2 m²	Rectangle` 	≃ 12 amp
Example 10	196 cm* 99cm	11	21.34 m²	Rectangle 	≃ 11 amp

Table 4: PV Integration achievements on prototype. (Source: Researcher)

Multi - functionality	PV modules on prototype used for several purposes like façade cladding elements, roof material, skylight/atrium cover, balcony railing or shadings.	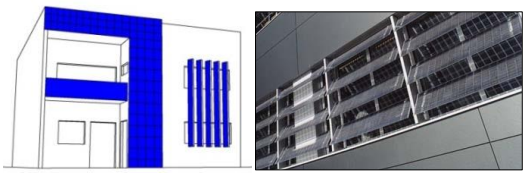
Shape and size	Flexible shapes (rectangle, square, curve, etc) and sizes (range from 0.2 to 2 m^2) are possible. The shape and size of the PV modules fit with the modular rhythm. The dimension of the modules can be customized to fit exactly on the facade without cut sizes.	
Color	It can be brown, blue or black, reddish brown, chocolate brown, hepatic and sage green colors.	
Material and surface texture	opaque modules have a homogeneous surface with fine lines, however the technology allows the possibility to produce semi-transparent modules with a variety of patterns (point, stroke, stripes)	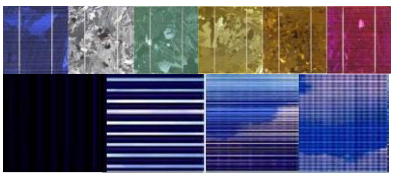
Flexibility in integration	With the small sized PV cells used, much freedom exists in integration, and since the most of facade is clad with PV, much freedom existed in the layout of integration.	
Types of Jointing	Jointing can be made through the aluminium framing, by integration into curtain wall systems with mullion/transom, or modules can be integrated frameless in glazing systems, with negative jointing. For roof applications, overlapping is often chosen for the horizontal joint. Custom made products can be developed too.	

Journal Home Page: https://sites.google.com/a/univsul.edu.iq/sjes

Review Article:

Direct shear strengthening of NSC and SCC using NSM CFRP and steel bars

Rozhno Omer Mustafa[1]
Mohamed Raouf Abdul-Kadir[1]

[1]University of Sulaimani, College of Engineering, Civil Engineering Department.

Article Inform

Article History:
Received 8 July 2019
Accepted 28 August 2019
Available online 1 June 2020

Keywords: Direct shear, NSM, Strengthening, CFRP rod.

About the Authors:
Corresponding author:
Rozhno Omer Mustafa - MSc.
E-mail: rozhnw.mustafa@univsul.edu.iq
Researcher Involved:
Dr. Mohamed Raouf Abdul-Kadir - Professor.

DOI Link: https://doi.org/10.17656/sjes.10126

Abstract

Failure in direct shear is sudden and catastrophic in concrete structures, Several techniques have been developed for shear strengthening of push-off specimens representing direct shear. In this research, the effectiveness of Near-surface mounted (NSM) FRP and steel bars as a strengthening technique for direct shear in normal strength concrete (NSC) and self-compacted concrete (SCC) are studied. As a result of the experimental work, it was observed that the NSM steel bars increased the shear capacity by 48 and 44% for both types of concrete NSC and SCC respectively, while the NSM CFRP rods increased the shear capacity by 30% and 33% for both NSC and SCC respectively. It was also observed that strengthening at 90° was more effective in terms of shear strength compared to 45° with a difference in the range of 8% for NSC and 5% for SCC. The analytical results are very close to the experimental ones.

1. Introduction

Employment of fiber reinforced polymer (FRP) composites to repair and retrofit concrete elements has been steadily increasing. The use of near surface mounted (NSM) fiber reinforced polymer (FRP) rods is a promising technology for increasing flexural and shear strength of deficient reinforced concrete members. Design of members for direct shear is usually made using shear friction method, which is accepted by the (ACI 318-14). If cracks occur in members subjected to direct shear there is a need for strengthening to avoid complete collapse.

Saenz N. et al. (2005) tested thirty-six internally unreinforced push-off specimens cast using

concrete with $f'_c = (34 - 37)$ MPa. They used CFRP laminate for strengthening in three groups and four CFRP ratios of 0.31%, 0.62%, 0.82% and 1.23%. The average shear load enhancement was 74.86%, 66.75%, 67.67% and 65.2% for the four ratios, respectively. They observed that the three strips of CFRP (with the same CFRP ratio) provided greater load enhancement compared to the other wrapping scheme. The shear friction strength of un-cracked concrete externally reinforced with CFRP composites ranged from 0.17 f'_c to 0.27 f'_c.

Zangana B. A. M. (2008) tested 27 unreinforced push-off specimens, with average f'_c of 34 MPa. The specimens of the first group were strengthened with one, two and three layers of GFRP at 90° and 45°. The same number of specimens in another group were strengthened using CFRP laminate. For 45° inclined strips the shear strength performance of GFRP was better than that of CFRP. The strengthened specimen with CFRP at 90° provided more shear strength compared to those specimens strengthened with the same CFRP strips at 45°. He concluded that CFRP strips had more significant contribution on shear strength enhancement compared to GFRP strips.

Jayaprakash J. et al. (2009) investigated the shear transfer capacity and mode of failure of reinforced concrete pre-cracked push-off specimens bonded externally with a layer of bi-directional CFRP sheets. The shear reinforcements ratio provided across the shear plane were (0.14%, 0.28% and 0.42%) and a concrete with $f'_c = 30$ MPa was used. They concluded that when the internal shear reinforcement increased, the contribution of CFRP laminate on the shear enhancement is reduced. The results indicated that shear displacement was significantly low for strengthened specimens, but there was a sudden increase in a shear slip at the peak load.

Shariatmadar H. et al. (2013) conducted tests on six pre-cracked push-off concrete specimens with $f'_c = 37$ MPa. The specimens were divided into two groups both with ρ_v = (0.92%, 1.23% and 1.54%). One group was not strengthened but the other was strengthened externally with two layers of 140 mm wide CFRP strips (ρ_f = 0.35%). The shear strength was increased by 5.24% for the specimens strengthened with two layers CFRP strips. The contribution of CFRP laminate on the shear strength reduces when the amount of internal steel reinforcement increases.

Naserian R. et al. (2013) study included testing of 16 non-cracked push-off specimens internally reinforced with steel reinforcement with ratios between zero and 1.54% and externally strengthened with different widths of Glass FRP layers (0,90,140 and 240 mm). In the strengthened specimens, shear transfer capacity increased from 3% to 38% compared to non-strengthened specimens. The contribution of FRP reinforcement in shear transfer capacity, as the percentage of cylindrical concrete strength (f'_c), was between 0.6% f'_c and 3.7% f'_c.

Fattah O. A. (2016) conducted tests on twenty push-off specimens with (0, 0.0067, 0.01 and, 0.0134) shear reinforcement ratio. The strengthening was made with one or two layers of CFRP. The test results showed that the contribution of CFRP laminates and their ratio were more effective for non-reinforced concrete compared to reinforced concrete subjected to direct shear. The shear strength enhancement compared to control specimens were 1.91, 1.29, 1.18 and 1.17 for the four shear reinforcement ratios respectively.

2. Research objectives

The main objectives of this research are to study shear strength modes of failure and deformation behavior of push off specimens subjected to direct shear after strengthening using different materials and methods, focusing on the NSM technique with FRP and steel bar applied in

different configurations. The techniques are applied on two types of concrete with similar compressive strength namely NSC and SCC.

3. Materials and Experimental Work

3.1 Experimental Program

Twenty push- off concrete specimens with the same shear reinforcement ratio of ρ_v = 0.013 were tested, with dimensions as shown in Fig.1. The specimens were classified into two group, with ten specimens each, the first group was cast with normal strength concrete (NSC) and the second group was self-compacted concrete (SCC). Then each group is classified as control, strengthened with CFRP rod and strengthened with steel bar as summarized in Table 1.

3.2. Materials

The materials used in experimental works were necessary to prepare normal strength concrete (NSC) mix and self-compacted concrete (SCC) mix with a designed cylinder compressive strength of 50 MPa using Ordinary Portland Cement (Type I) from Tasluja company. Natural sand from Darbandikhan area was used as fine aggregate with grading conforming to (ASTM C136, 2014) with specific gravity = 2.64. Natural gravels from Goptapa region with nominal maximum size (19 mm) was used for the NSC, however, course aggregate grade of (Max. size Agg. =12.5 mm) was used for the self-compacting concrete. Deformed steel bars of Ø 8 mm diameter with $f_y = 384$ MPa and $f_u = 531$ MPa was used as shear reinforcement and for strengthening purposes, steel bar of Ø 16 mm with $f_y = 522$ MPa and $f_u = 648$ MPa was used for L-shaped parts of push-off specimens.

High-Performance Superplasticizer admixture was used in the production SCC mix to improve workability and increase ultimate strength. The external strengthening material was carbon fiber reinforced polymer (CFRP) rebar with tensile strength $f_u = 2000$ MPa was used with adhesive epoxy resin (Sikadur-330) to place CFRP rods in the groove of the concrete surface for the NSM technique.

The properties of the concrete are summarized in Table 2. The mix proportions of SCC satisfy the criteria of filling ability and segregation resistance, specified by L-box, V-funnel and slump flow. These tests were conducted to ensure the suitability of the mix. The testing apparatus is shown in Figure 2 and the results are shown in Table 3 (EFNARC Guidelines., 2005).

3.3. Specimen Preparation

The molds for the specimens were designed to be erected easily and made of two parts from the galvanized steel plate of 3 mm thickness. The two parts were connected with screws and bolts in two opposite corners. The specimen mold was connected tightly to a plywood base using fast screws. The materials for each batch were prepared by weight, then mixed in an electrical tilting mixer of (0.08 m^3) capacity. The mixing operation was continued until workable concrete was obtained.

The concrete was then poured into the forms with the steel cage inside in two-layer and each layer for (NSC) was vibrated for about 30 seconds. Along with each group, six cylinders (300 mm * 150 mm) were cast as a control for compressive strength of concrete and six cylinders (200mm*100mm) were cast for splitting tensile strength of concrete.

3.4. Strengthening process with CFRP rod and steel bar using NSM technique

The following steps were carried out during strengthening process:

On the surface of the concrete, grooves were cut by hand cutting and hammer drilling machine

after marking the layout. The grooves were cleaned and brushed dust free before working on it, the epoxy resin mixture was applied and half-filled the grooves. The CFRP rod or steel bar was placed inside the groove and pressed lightly to be fixed, then the groove was filled with resin and the surface was leveled. The grooves on the surface were cut at 90° angle (perpendicular to the shear crack plane) and at 45° angle for strengthening the specimens as shown in fig. 3.

3.5. Testing procedure

All specimens were tested under a single point loading. Loading was applied through a controlled hydraulic operated jacking with a maximum capacity of (700 kN), fixed to the loading frame as shown in Fig.4. the instrumentation was so arranged to apply the load at the center of the specimen without eccentricity and to prevent local failure. The load was applied gradually with 10 kN increments till failure at the shear plane.

The vertical displacement which represents the slip along the shear plane and the lateral displacement that represent the cracking width in the push-off specimens were measured using three linear variable displacement transducer (LVDT) with (0.001 mm) precision, two at the front for indicating the crack width and one for the slip in the other sides of the specimen. Electrical resistance strain gauges of (0.01 mm) accuracy with P-3500 digital strain indicator were used to measure the tensile strain in the steel and CFRP rods and compression strain in the concrete. The control cylinder specimens were tested using the compression testing machine of 3000 kN capacity.

4. Results and Discussion

Results of concrete compressive strength obtained from the control cylinder specimens, the ultimate and first crack load, shear strength, first crack load ratio (strengthened/control) and shear strength ratio (strengthened/control) for all the tested push-off specimens are presented in Table 4.

4.1. Behavior of the Push-off specimen

A comparison is made between the control specimen and the strengthened ones for each group in terms of mode of failure, cracking and ultimate loads, displacement and strain.

4.1.1. Modes of failure

As loads were applied gradually, the shear cracks appeared near the shear plane and by increasing loads the cracks propagated toward the center of the shear plane. Failure in the control specimens (C1 and D1) initiated with cracks occurred at both sides along the shear plane, these cracks extended and well-observed until reaching failure load. Even though cracking occurred, the L-shaped parts of the push-off specimens did not split completely because of the presence of shear reinforcement across the shear plane. However, at the final failure of the specimen the L-shaped parts split apart without rupture of the shear reinforcement as shown in Fig.5.

For the remaining specimens, the failure of the specimens strengthened at both 45° and 90° initiated at the strengthening area at the same angle of the bars at the weakest point (between bars). The final failure was debonding of the bars by splitting of the concrete cover and cracking of the surrounding concrete, associated with the diagonal tension failure of concrete. This mode of failure was more obvious in the specimens strengthened at 90° angle as shown in Figs. 6 and 7. This type of failure may be prevented by providing better anchorage of the NSM bars crossing the critical shear crack, either by anchoring the bars into the concrete shear plane

or using bars fully wrapped bars around the specimen.

4.1.2. Cracking and ultimate loads

Reforming to Table 4, the results show that the presence of NSM CFRP and steel bars increases the first cracking load. The ratio of cracking shear strength of CFRP strengthened specimens to control specimens are 1.12 and 1.36 for NSC for C2 and C3 respectively, and for SCC the values 1.06 and 1.24 for D2 and D3 respectively, however, for the steel strengthened specimens the ratios are 1.36 and 1.49 for NSC for C4 and C5 respectively, and 1.12 and 1.41 for SCC for D4 and D5 respectively. The cracking ratios in strengthened steel bar specimens are higher compared to CFRP specimens.

In the internally reinforced specimens when cracking initiates along the shear plane, the shear reinforcement provided across the crack support the extra shear stresses as clamping force till the steel reinforcement yields. As seen from Table 4, for normal strength concrete specimens (Group C), the ratio of shear strength after strengthening with CFRP rods at 45° and 90° (C2 and C3) were 1.26 and 1.36 respectively. However, the shear strength ratios were equal to 1.43 and 1.52 for steel bar strengthening at 45° and 90° respectively. For the self-compacted concrete group D specimens, the shear strength of the specimen strengthened with CFRP rods compared to D1 have increased by 1.30 and 1.35 for (D2 and D3) for 45° and 90° inclinations respectively. For specimens D4 and D5 strengthened with steel bars the increments were 1.40 and 1.47 times the control D1. This indicates that the steel bars were performing better than CFRP bars for both inclination arrangements and for both types of concrete. The ultimate shear strength in SCC (group D) is higher than in NSC (group C) due to the high tensile strength in SCC. Although the shear strength enhancement is moderate, the process of strengthening concrete using CFRP rod or steel bar is acceptable.

4.2. Deformation characteristics

4.2.1. Slip

At the beginning of cracking the slip between the two halves of the specimen as measured by the vertical LVDT occurred as a result of the compression of the inclined concrete struts between reinforcement crossing the shear plane. The component of this compression parallel to the shear plane is referred to slipping when discussing its behavior.

Fig.8 shows the shear stress - slip relationship of the specimens strengthened with different strengthening materials and angle of configuration. It is noticed that strengthening with steel bars at 90° (C5 and D5) reduced the amount of the slip in the specimens more than other specimens at same stress value for both NSC and SCC, the reason may be due to effect of strengthening technique inclination. Figure 9 shows the slip at failure for Group C and Group D. The figure shows that the slip at failure in group C (NSC) specimens is lower than that in Group D (SCC) specimens. Hence Group C showed an increase in stiffness, but failed in a brittle manner.

4.2.2. Crack width

The shear stress and crack width relationship of the strengthened and un-strengthened specimens are shown in Fig. (10). The figures show that the strengthened specimens showed a smaller value of shear displacement and crack width at failure load compared to un-strengthened specimens. The specimens with bars placed at 90° angle such as C3, C5, D3, and D5 exhibited less crack width compared to other specimens because the bars are perpendicular to the cracks. Fig.11 shows Crack width at failure for Group C and Group D specimens, the figure shows that group D specimens exhibited

low crack width compared to group C, this may be because in normal strength concrete (Type C) the bond strength between mortar and aggregate particles is low, cracks generally propagate around the aggregate particles, producing a rough surface, while in Self-compacted concrete (Type D) the bond strength between mortar and aggregate particles is apparently greater, as indicated by the splitting tensile strength for NSC and SCC are (4.67 and 5.16 MPa) respectively.

4.2.3. Strain in concrete, steel and CFRP bars

The maximum compression strain of concrete at the surface of the shear plane terminates at the end of loading. It should be noted that this strain is related to clamping stress. Fig.12 shows the shear stress relationship with a concrete strain of the un-strengthened and strengthened specimens. It is noticed that the concrete strengthened with a steel bar at 45° has the maximum strain amount compared to all of the other specimens for both NSC and SCC. Fig.13 shows the comparison of concrete strain for group C (NSC) and group D (SCC) specimens. It can be noticed that the strain for both groups is too close with a small difference which is higher in group D at the same load especially at large shear stresses.

Fig.14 show the results of tensile strain in the stirrups for the strengthened specimens. The figure shows that the strain in stirrups in strengthened specimens is much smaller than in non-strengthened specimens. This may be the effect of the strengthening technique which reduces load transfer to the stirrups, and shear reinforcement dowel action is minimized in contrary to non-strengthened specimens. Fig.15 shows the shear stress-strain in stirrups relationship for Group C and Group D, which shows that internal shear reinforcement strains in both NSC and SCC are the same until reaching high shear stress at which group D exhibit higher strains in their stirrups due to the high shear strength of this

The shear stress-strain for strengthening materials in group C and D specimens are shown in Fig. (16). After concrete cracking, the steel and CFRP rods are strained. However, after their peak shear stress is reached, the strengthening materials debonded rapidly and consequently, the strain dropped. Based on the results, strain in steel bar was smaller than that in the CFRP rod, due to a higher bond between the deformed steel bars and epoxy resin the NSM technique.

The strain in steel bars for group C (NSC) was approaching yield strain. Fig. (17) shows the shear stress–strain relationship for strengthening materials in Group C and Group D, the figure shows that group D (SCC) specimens exhibited low strain compared to group C (NSC), this may be due to the high tensile strength in SCC.

5. Theoretical analysis

In this section some of present models for shear strength prediction are presented and from the data collected from tests and using regression analysis a new model for direct shear strength of concrete strengthened with NSM technique is proposed.

5.1. Present models for direct shear strength prediction

Mattock, A. H. (2001) proposed simple equations for shear friction design, which allow the full potential shear transfer strength of concrete to be utilized. This equation is expressed as follows:

$$v_n = 0.1\, f'_c + 0.8\, \rho_v f_y \qquad \text{Eq. (1)}$$

Where f'_c is concrete strength and not more than 55 MPa, f_y = yield stress of shear friction reinforcement and ρ_v = internal reinforcement ratio.

Saenz N. et al. (2005) presented an equation to determine the concrete shear friction strength and the additional shear friction strength provided by the concrete–CFRP interaction, the relation between ultimate shear to concrete compressive strength, v_u/fc' versus effective CFRP composite tensile stress normalized by the concrete compressive strength is calculated and the line of best fit is

$$v_u = 0.117\, fc' + 0.505\, \rho_f f^* f_u \qquad \text{Eq.(2)}$$

Where $\rho_f f^* f_u$ is the effective CFRP composite tensile stress, which is the clamping stress provided by the CFRP composite.

Mohammed A. A. et al. (2012) for the case of unidirectional CFRP laminate obtained the following equation from regression analysis for the shear enhancement of plain concrete after strengthening.

$$\Delta_{vn} = 0.069\left(\rho_f f_f + \rho_{fi} f_{fi} cos\alpha\right)^{1.177} \qquad \text{Eq.(3)}$$

In which Δ_{vn} is the shear strength enhancement, ρ_f is the ratio of CFRP layer in the concrete section perpendicular to the shear plane, f_f is the fracture tensile stress in CFRP material, ρ_{fi} is the CFRP ratio of the inclined strips provided to the section and α is the angle of inclined strips measured from shear plane, and f_{fi} is the fracture tensile stress of the lettered CFRP laminate. The shear strength of strengthened concrete is that of plain concrete plus that obtained from the value obtained from the above equation multiplied by the basic shear strength.

Naserian R. et al. (2013) obtained three equations for calculating direct shear strength of non-cracked concrete strengthened with GFRP laminate, for three steel reinforcement parameter ($\rho v\ fy$) equal to 3.3, 4.4 and 5.5 MPa. Later, a refined equation for all reinforcement ratios having the following form was obtained from a regression analysis

$$v_u = 0.116\, f'_c + 0.803\, \rho_v f_y + 0.144\, \rho_f f_{fu} \qquad \text{Eq.(4)}$$

Where ρ_f = external reinforcement ratio, f_{fu} = ultimate tensile strength of FRP strip.

Fattah O. A. (2016) proposed equation for shear strength for plain and reinforced concrete, strengthened with CFRP laminate or GFRP laminate based on 20 specimen which were classified into four groups, according to shear reinforcement ρυ (0, 0.0067, 0.01, and 0.0134. After regression analysis the final equation for the shear strength was

$$v_n = 0.132\, f'_c + 0.636\, \rho_v f_y + 0.389\, \rho_f f_{fu^*} \qquad \text{Eq.(5)}$$

In which ρ_f = external reinforcement ratio, f_{fu^*} is the composite tensile strength of the laminate.

5.2. Prediction of Direct Shear Strength of Concrete with NSM bars

Based on the properties of concretes with different type of strengthening materials and degree of orientation for strengthening technique, an equation is proposed for shear strength of concrete strengthened with NSM bars. Since type of concrete and degree of bar inclinations are different in each group, the shear transfer capacity is computed by adding another term to consider the contribution of FRP rod (v_f) and external steel bar (v_{se}). This equation is expressed as following:

$$v_u = a^*\left(b\, fc' + c\, \rho_v f_y + d\, \rho_f f_{fu} * \sin\alpha + e\, \rho_v f_{su} * \sin\alpha\right) \qquad \text{Eq.(6)}$$

Where: a^* = coefficient for type of concrete (NSC and SCC), b = concrete cohesion coefficient; c = concrete–stirrup shear friction interaction

coefficient; d = concrete–FRP shear friction interaction coefficient; e = concrete–external steel bar shear friction interaction coefficient; α = degree of inclination strengthening material in NSM technique (45° and 90°); f_{fu} = ultimate tensile strength of the CFRP rod; f_{su} = ultimate tensile strength of the steel bar. A linear regression analysis was used for the test results and the final equation for the direct shear strength is :

$$v_u = a^* (0.120\, fc' + 0.800\, \rho_v f_y + 0.757\, \rho_f f_{fe} * \sin\alpha + 2.106\, \rho_v f_{se} * \sin\alpha) \quad \text{Eq.(7)}$$

Where : $a^* = 1\ for\ NSC\ and\ \ a^* = 1.081\ for\ SCC$

The correlation coefficient (R^2) for the above relationship is 0.95 while the mean value (test / predicted) is 1.01 and standard deviation is 0.25 as shown in Fig.18. These values indicate that there is a valid agreement between the test results and the predicted shear strength. When this equation is applied to result of past models (Mattock, A. H., 2001, and others), and including this research, the mean (test / calculated) shear strength based on the proposed equation is equal to 0.90, and standard deviation is 0.33 as shown in Fig.19.

6. Conclusions

Based on the experimental and analytical investigations, the following main conclusions can be drawn:

- NSM strengthening technique with CFRP bars (6 mm diameter) for reinforced push-off specimens increase the shear strength capacity by 1.31 and 1.33 for NSC, and SCC respectively.
- The increments for the NSM steel bars with (8 mm diameter) were 1.48 and 1.44. The NSM technique was more effective for steel bars.
- The ultimate shear load capacity increment for shear strengthening in NSC is a little higher than in SCC when using the same strengthening techniques.
- The strengthening by CFRP rods and steel bars at a 90° angle were more effective in terms of maximum load-carrying capacity compared to 45° angle, the difference was in the range of % 8 for NSC and % 5 for SCC in reinforced specimens.
- The conventional steel bars strengthened specimens showed a slightly more favorable response than those strengthened with CFRP rod to direct shear strength by 1.13 for NSC and 1.09 for SCC specimens.
- In the un-strengthened specimens, the cracks occurred along the shear plane until reaching failure load. However, for the strengthened specimens, the failure occurred at the same angle of strengthening rods at the weakest region (between rods) and debonding happened in all the specimens as indicated by stripping off the strengthened part.
- The shear displacement (shear slip) and crack width of the strengthened specimens were less compared to the un-strengthened specimens for the same load. However, there was a sudden increase as the load reaches its peak.
- At maximum load, the crack width in the NSC was 2.6 mm compared to 2.2 mm for SCC specimens.
- The maximum vertical displacements (shear slip) were 9.5 mm and 8.8 mm for NSC and SCC specimens respectively.
- The proposed model equation showed good results when applied to the experimental results of this investigation and others experimental results.

تقوية القص المباشر للخرسانة العادية والخرسانة ذاتية الرص باستخدام قضبان ألياف الكربون البوليمرية والحديد مثبتة قرب السطح

رۆژنۆ عمر مصطفى[1] - ماجستير
د. محمد رۆوف عبدالقادر[1] - استاذ

[1] جامعة السليمانية ، كلية الهندسة ، قسم الهندسة المدنية

المستخلص

الفشل عند قص المباشر للمباني الخرسانية يكون مفاجئا وخطراً. لقد تم تطوير العديد من طرق التقوية لنماذج تخص القص المباشر. الهدف من هذا البحث كان دراسة تأثير تقنية التقوية عن طريق وضع القضبان قريبة من سطح الخرسانة لنماذج من خرسانة العادية المقاومة والخرسانة ذاتية الرص. قد بينت نتائج الفحوصات بأن التقوية بقضبان ألياف الكربونية تزيد من مقاومة القص المباشر بنسبة 30% و 33% للخرسانة العادية وذاتية الرص على التوالي حيث كانت الزيادة 44% و 48% عند استعمال قضبان الحديد للتقوية. كما وإن استعمال تقنية NSM تقلل من عرض الشقوق و كمية الانزلاق والتشوه الحاصل في قضبان القص الداخلي. كما واظهرت النتائج بأن التقوية بزاوية 90 لكلا النوعين من القضبان العطت مقاومة قص اكبر من النماذج المقواة بزاوية 45 بنسب تتراوح من 8% الى 5% للخرسانة العادية والخرسانة ذاتية الرص على التوالي. التحليلية قريبة جدا من النتائج التجريبية.

الكلمات المفتاحية : القص المباشر ، NSM ، التقوية ، CFRP ، الخرسانة العادية ، الخرسانة ذاتية الرص.

References

1- American Concrete Institute. (2014). Building Code Requirements for Structural Concrete (ACI 318-14): Commentary on Building Code Requirements for Structural Concrete (ACI 318R-14): an ACI Report. American Concrete Institute. ACI.
2- ASTM C136. "Standard Test Method for Sieve Analysis of Fine and Coarse Aggregates.", Annual Book of ASTM Standard, Vol. 04, October 2014.
3- EFNARC Guidelines. (2005). The European Guidelines for Self-Compacting Concrete; Specification, Production and Use. p. 63.
4- Fattah, Omed Amin (2016). "Strengthening concrete for Direct Shear." MSc. thesis University of Sulaimani.
5- Jayaprakash, J., Samad, A. A. A., & Abbasvoch, A. A. (2009). Experimental Investigation on Shear Capacity of Reinforced Concrete Pre-cracked Push-off Specimens with Externally Bonded Bi-Directional Carbon Fiber Reinforced Polymer Fabrics. *Modern Applied Science*, *3*(7), 86-98.
6- Mattock, A. H. (2001). Shear friction and high-strength concrete. *Structural Journal*, *98*(1), 50-59.
7- Mohammed, A. A., & Hassan, G. B. (2012). Prediction of Load Capacity of Reinforced Concrete Corbels Strengthened with CFRP Sheets. *World Academy of Science, Engineering and Technology, International Journal of Civil, Environmental, Structural, Construction and Architectural Engineering*, *6*(8), 563-568.
8- Naserian, R., Hosseini, A., & Marefat, M. S. (2013). Assessment of shear transfer capacity of non-cracked concrete strengthened with external GFRP strips. *Construction and Building Materials*, *45*, 224-232.
9- Saenz, N., & Pantelides, C. P. (2005). Shear friction capacity of concrete with external carbon FRP strips. *Journal of structural engineering*, *131*(12), 1911-1919.
10- Shariatmadar, H., Khatamirad, M., & Zamani, E. (2013). Pre-cracked concrete shear strengthened with external CFRP strips. Journal of rehabilitation in civil engineering, 1(1), 29-38.
11- Zangana, Bakhtiar Aziz (2008). "Effect of wrapped R.C beams by carbon and glass Fiber strips internally and externally to the Shear Capacity." MSc. thesis University of Mosul.

Table 1: Details classification of push off specimen. (Source: Researcher)

Group		Type of concrete	Technique of strengthening	Strengthening material	Degree of inclination
C	C1	Normal Strength Concrete	Control	Not strengthening	---------
	C2		NSM	CFRP rode, 6 mm	45 °
	C3		NSM	CFRP rode 6 mm	90 °
	C4		NSM	Steel bar, 8 mm	45 °
	C5		NSM	Steel bar, 8 mm	90 °
D	D1	Self-Compacted Concrete	Control	Not strengthening	----------
	D2		NSM	CFRP rode, 6 mm	45 °
	D3		NSM	CFRP rode 6 mm	90 °
	D4		NSM	Steel bar, 8 mm	45 °
	D5		NSM	Steel bar, 8 mm	90 °

Table 2: Mix compositions of NSC and SCC. (Source: Researcher)

	Materials (Kg / m^3)							
Type of Concrete	Cement	Fine Agg.	Coarse Agg. Max. 19 mm	Coarse Agg. Max. 12.5 mm	Water	S.P	W / C	Mix Proportion C : S : G
Normal Strength Concrete (NSC)	500	870	1190	_____	210	0	0.42	1:1.74:2.38
Self-Compacted Concrete (SCC)	465	1380	_____	1000	158	6.32 (% 1.36)	0.34	1:2.97:2.15

Table 3: SCC properties requirements as per EFNRC 2005. (Source: Researcher)

Method	Results	Minimum Range	Maximum Range
Slump flow (mm)	690	550	850
T 500 mm Slump flow (sec.)	8	2	9
V-funnel (sec.)	11	6	12
L Box (h2 / h1)	0.81	0.7	1.0

Table 4: Test Results. (Source: Researcher)

Group	Specimen designation	f'_c (MPa)	Splitting Tensile Strength (f_{ct}) (MPa)	First crack load (kN)	Ultimate load (P_u) (kN)	Ultimate shear strength (v_u) (MPa)	First crack load ratio (strengthened / control)	Shear strength ratio (strengthened / control)
C	C1	53.73	4.67	290	342	11.40	-	-
	C2			324	432	14.40	1.12	1.26
	C3			396	468	15.60	1.36	1.36
	C4			396	490	16.33	1.36	1.43
	C5			432	522	17.40	1.49	1.52
D	D1	51.14	5.16	306	360	12.00	-	-
	D2			324	468	15.60	1.06	1.30
	D3			378	486	16.20	1.24	1.35
	D4			342	504	16.80	1.12	1.40
	D5			432	530	17.66	1.41	1.47

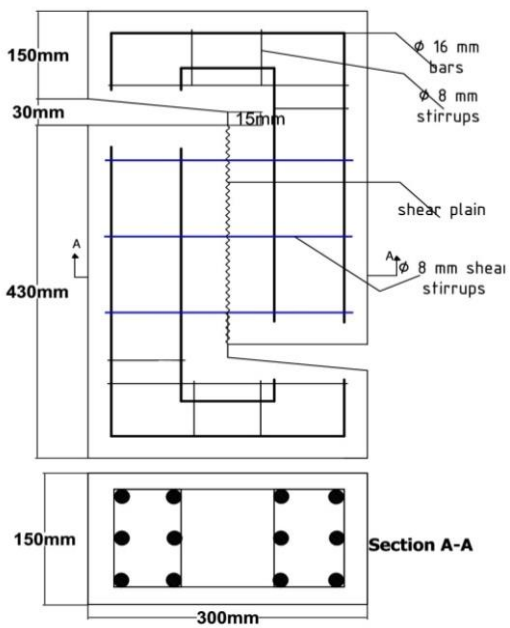

Fig.1: Detail of test specimen, ρυ = 0.013 , Aυ= 6 ø 8 mm bars. (Source: Researcher)

(a)

(b)

(c)

Fig. 2: Rheological parameters of the SCC: (a) Slump flow; (b) V-funnel; (c) L Box test (EFNARC Guidelines., 2005).

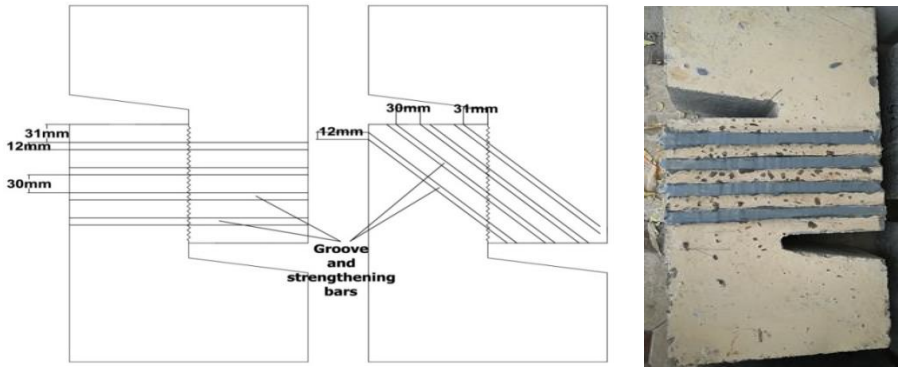

Fig. 3: Dimensions of the grooves for the strengthening bar and NSM technique. (Source: Researcher)

Fig. 4: Instrument and push off specimen that ready for test. (Source: Researcher)

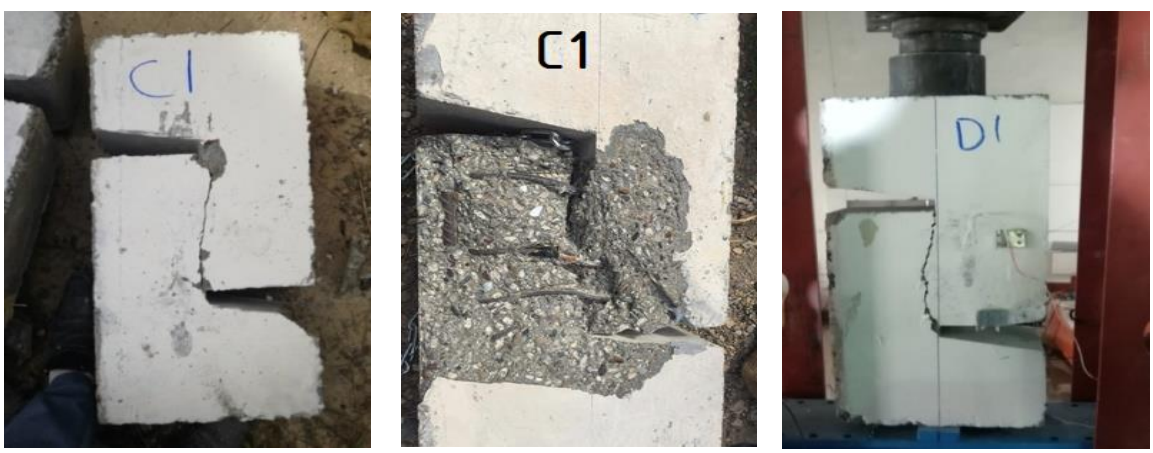

Fig. 5: Specimens C1 and D1 after failure. (Source: Researcher)

Fig. 6 : Specimens C2, D2, C4 and D4 after failure. (Source: Researcher)

Figure 7 : Specimens C3, D3, C5 and D5 after failure. (Source: Researcher)

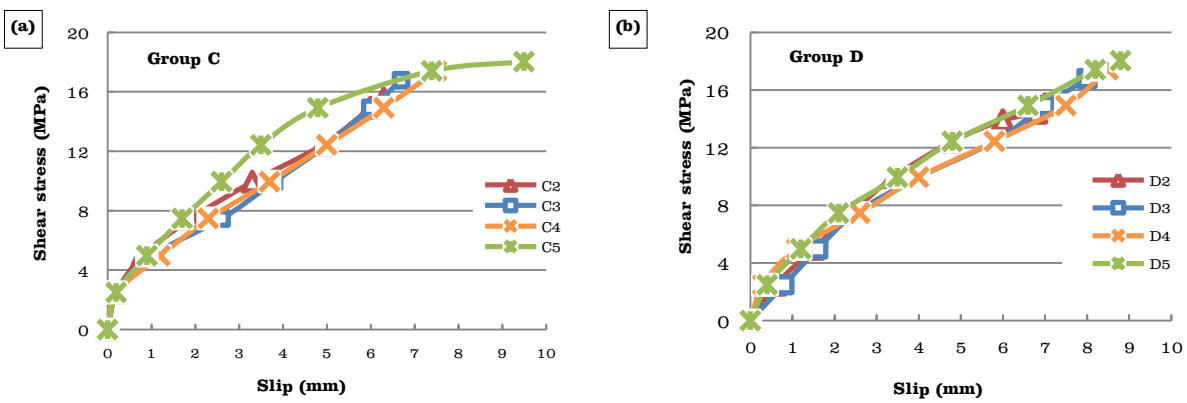

Fig. 8: Shear stress – vertical slip relationship: (a) Group C ; (b) Group D. (Source: Researcher)

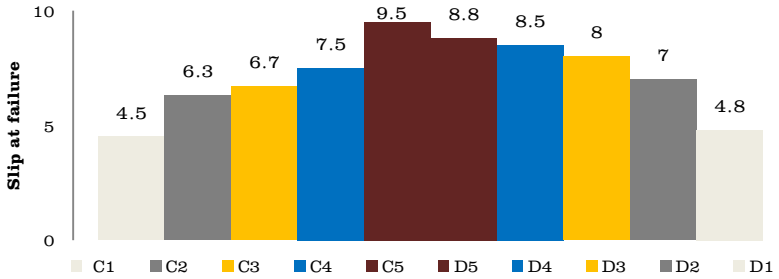

Fig. 9: Slip at failure for Group C and Group D. (Source: Researcher)

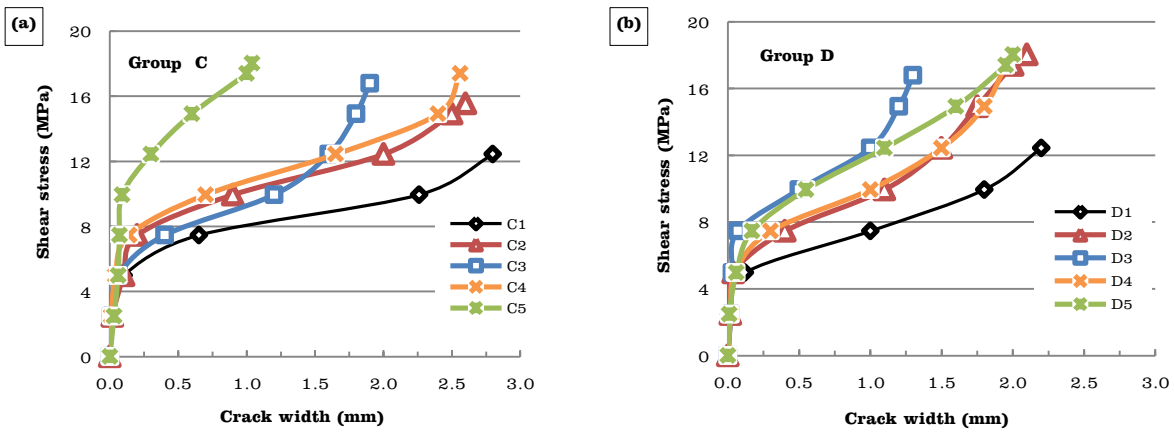

Fig.10: Comparison of Shear stress – Crack width relationship : (a) Group C ; (b) Group D . (Source: Researcher)

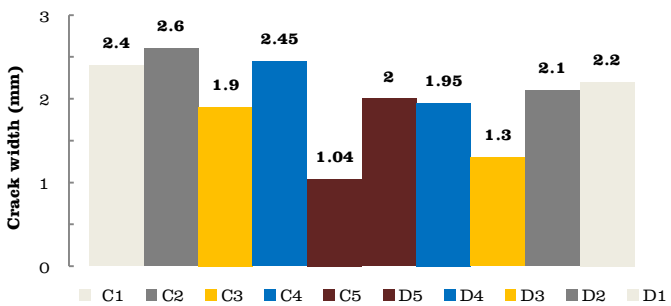

Fig. 11: Crack width at failure for Group C and Group D. (Source: Researcher)

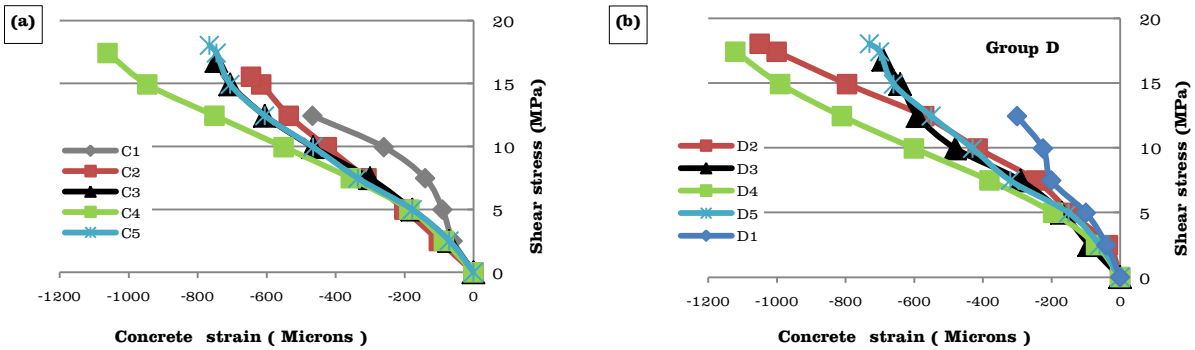

Fig. 12: Shear stress – Concrete strain relationships : (a) Group C ; (b) Group D. (Source: Researcher)

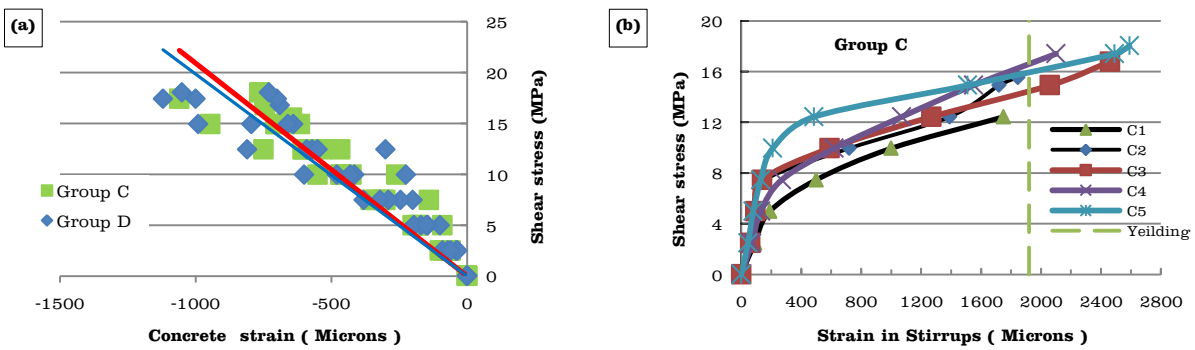

Fig. 13: Shear stress – Concrete strain relationship for Group C and Group D. (Source: Researcher)

(a)

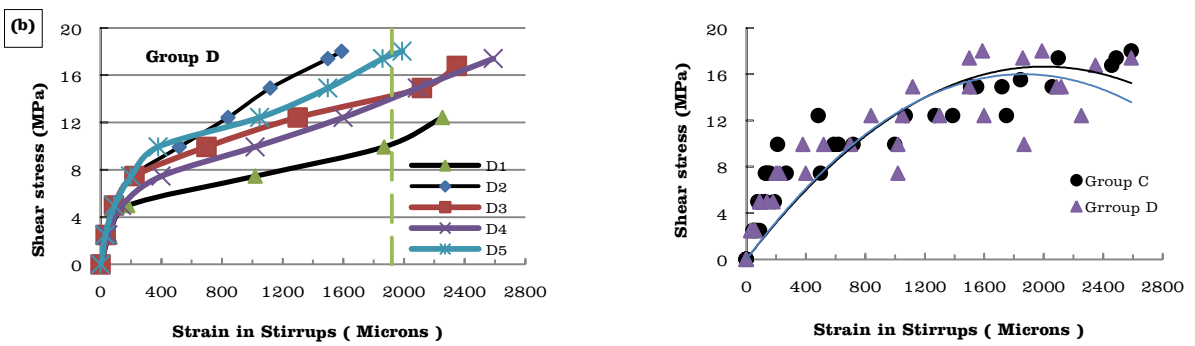

Fig. 14: Shear stress –strain in stirrups relationships : (a) Group C ; (b) Group D.
(Source: Researcher)

Fig. 15: Shear stress – Strain in Stirrups relationship for Group C and Group D.
(Source: Researcher)

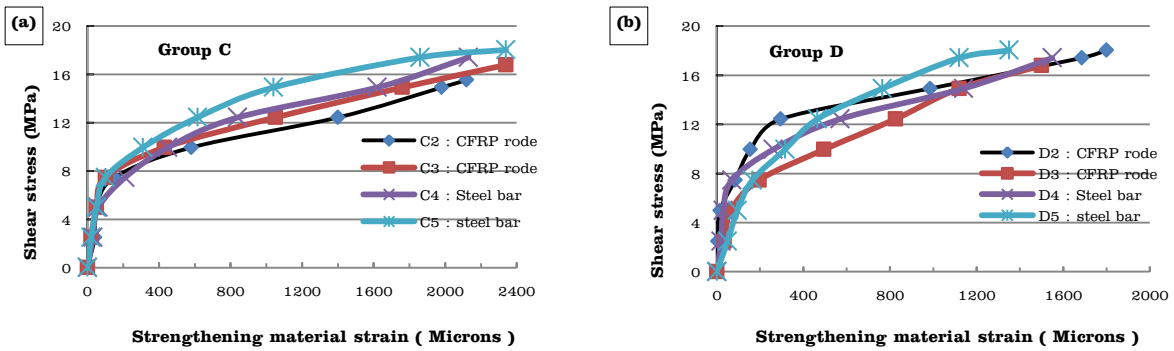

Fig. 16: Shear stress – Strengthening materials strain relationships: (a) Group C ; (b) Group D. (Source: Researcher)

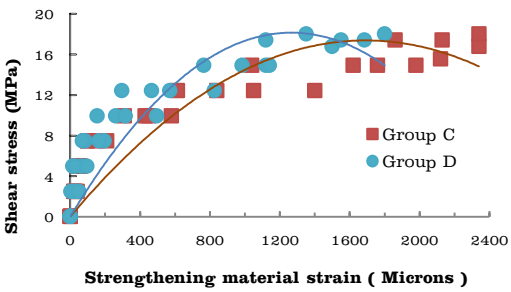

Fig. 17: Shear stress – Strengthening materials strain relationship for Group C and Group D. (Source: Researcher)

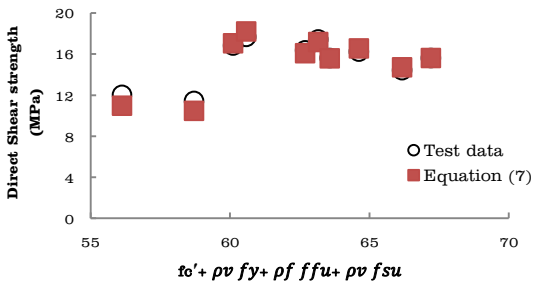

Fig. 18: Relationship between shear strength and predicted equation values. (Source: Researcher)

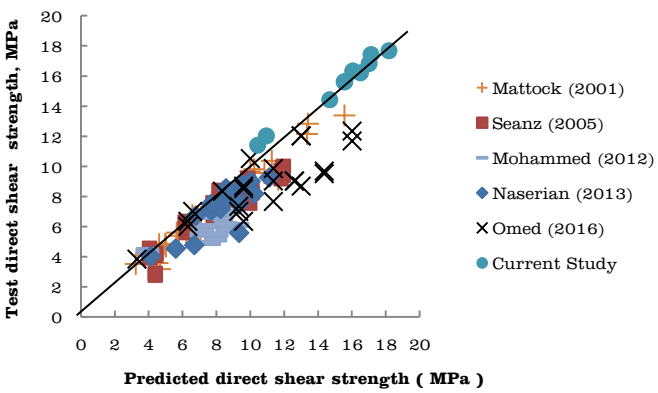

Fig. 19: Comparison of test and predicted results. (Source: Researcher)

Journal Home Page: https://sites.google.com/a/univsul.edu.iq/sjes

Review Article:

Effect of Using Different Types of Polymer on Shear Strength of Simply Supported High Strength Reinforced Concrete Beams

Saman Mustafa Kamal[1]
Jalal Ahmed Saeed[1]

[1]University of Sulaimani, College of Engineering, Civil Engineering Department

Article Inform

Article History:
Received 22 September 2019
Accepted 16 April 2020
Available online 1 June 2020

Keywords: Beams; Compressive strength; High strength concrete; Shear strength; polymer; Stirrups.

About the Authors:
Corresponding author:
Saman Mustafa Kamal– MSc.
E-mail: saman_ceng@yahoo.com
Researcher Involved:
Dr. Jalal Ahmed Saeed - Professor.

DOI Link: https://doi.org/10.17656/sjes.10127

Abstract

This work is an attempt to study shear behavior of high strength reinforced concrete (modified with different types of polymer) beams. Fourteen simply supported reinforced concrete beams under central load in two groups are tested (with and without stirrups). All beams have the same cross section of (300x200) mm, length of 1200mm with the same reinforcement. The main variables were the compressive strength, shear reinforcement, types, and percentages of the added polymer to study the shear behavior of beams.

It has been found that by adding different types of polymer (powder and liquid) up to 1%, causes a reduction in water to cement ratio (w/c) from 0.35 to 0.23. The powder polymer improves the compressive strength for 39%, increasing of the splitting tensile strength (fsp) was 40%, improving the flexural strength (fr) was 64%.Whereas, the range of growth by using liquid polymer in compressive strength was 16%, increasing of the splitting tensile strength (fsp) was 16%, improving of the flexural strength (fr) was 59%. From these results and based on statistical analysis, a mathematical model has been drawn for high strength concrete modified with different types of polymer.

1. Introduction

One of the main challenges facing the civil and construction engineering community is to modify cement quantity in mix design by admixtures to enhance the mechanical properties [1]. For years, researchers have tried to find more useful materials and ways for decreasing the disadvantages of concrete and making the use of concrete more effective by adding admixtures for improving the properties of concrete in structural design [2]. Several experimental types of research have shown that the different percent of fly ash (FA) and silica fume (SF) are most common additives have been used to improve the properties of high strength concrete, which decrease the

cement content to reduce the cost, enhances the performance, mechanical properties, and durability of normal (NSC) and high strength concrete (HSC) in the hardened state [3, 4, 5]. Based on ACI 363 R, high strength concrete has a particular compressive strength of at least 55 MPa at 28 days [6,7].

Shearing force exists in beams due to change in bending moment along the span, so this force is equivalent to the rate of change of bending moment [8]. In a reinforced concrete member, flexure and shear combine to create a biaxial state of stress. Cracks form when the principal tensile stresses exceed the tensile strength of concrete. In a region of large bending moment, these stresses are greatest, at the external tensile fiber of the member, and they are responsible for the initiation of flexural cracks perpendicular to the axis of the member.

In the region of high shear force, significant principal tensile stresses, also, referred to as diagonal tension, attempt generated at approximately 45° to the axis of the member. These may result in inclined (diagonal tension) cracks [9]. To overcome shear failure web reinforcements are provided which has three primary effects on the shear strength of a beam [10], it carries a part of the applied shear force, and it restricts the growth of diagonal tension crack width, it ties the longitudinal bars and increases dowel action. In addition to these three actions, stirrups may transfer a small force across the crack by dowel action, and they tend to enhance the strength of the compression zone by confining the concrete.

The limited experimental work on the high strength concrete makes it difficult to safely predict the shear capacity of reinforced concrete members which is now evaluated based on of empirical equations proposed by different design codes with some modifications in the equations for normal strength concrete. Most of these equations are derived based on of experimental data of concrete with low compressive strengths, 40 MPa or less. Therefore, their application to higher values of compressive strength requires more extensive researches.

2. Objectives

a. Study the effects of different types of polymer on the physical and mechanical properties of high strength concrete.

b. To investigate the shear behavior of high strength reinforced concrete beams.

c. To compare the ultimate diagonal cracking shear strength obtained from test results with values calculated from ACI and other researcher's predictions.

d. To obtain an equation to predict the shear strength of high-strength reinforced concrete beams

3. Experimental Program

In this work Fourteen reinforced concrete beams with and without stirrups modified with different types of polymer, were cast and tested as a simply supported beam under concentrated load in the center. The beam specimens were separated into two groups according to the existing of stirrups or not. Each group comprised of seven beams as shown in Table 1.

4. Material

Ordinary Portland cement of Gasin brand was used (locally available 53 grade), the physical properties and chemical composition, according to ASTM C150 [10] are shown in Tables 2 and 3. Natural river sand was used as fine aggregate. The sand grading conforms to the limits of ASTM C33 [11]. Locally available coarse aggregate conforming to the graded aggregate of nominal size 9.5 mm maximum used which conforms to limits of ASTM C33 [11]. Two types of Synthetic powder besides two liquid polymer-based on reactive polymers were used. The commercial names of the two powder polymers are DBC-21(B), and VK-98 (F), while the commercial names of the two liquid polymers are SP633T (L2), and SIF N PUL (L4), the properties of the powder and liquid polymers are summarized in Tables 4 and 5. Deformed steel bars with two different diameters (8 and 16) mm used which found fy 481MPa. All steel bars were tested at the laboratories of (Gasin Cement Company), conforming to ASTM A615/A615M-09[12] specifications.

5. Concrete Mix Design

Several mixes originally are considered. The final mix used by weight is 1:1.5:2.5 (cement: sand: gravel) with water-cement ratio of 0.35 and the slump of almost 150mm for concrete (0% additive) and above 200mm for concrete with the polymer. All specimens were cured in water up to 28 days.

6. Specimen Details

Testing was carried out on 14 beams that were divided into two equal main groups, the first group was seven beams with stirrups and the others without stirrups, simply supported ends with a total span of 1200 mm, under one point concentrated load. All the beams have a constant cross section of (300x200) mm. For all beams, the bending reinforcements (3Ø16mm) was kept constant, for the beams with shear reinforcements (Ø8 mm @125mm) was selected to be in acceptance with ACI-318 [13], the details are shown in Fig. 1.

7. Test Procedure

All beams were tested after 28 days of age. Four electrical (LVDT)s of the type LD621-30 with 0.00001mm accuracy were used, for measuring web shear crack width, and deflection were fixed on the left side, center, right side and bottom of the beam as shown in Fig.2. All specimens were tested as a simply supported and loaded by a concentrated load at mid-span. At each load increment, mid-span LVDT readings for deflection and (LVDT)s readings for web shear crack width at both sides of the beams were recorded, position, load magnitude, and cracks which appeared were marked and recorded carefully, and these procedures were continued until failure. Along with each beam, the compressive strength ($f_c^`$) and the splitting tensile strength (f_{sp}) tests were carried out on standard (150*300) mm cylinder specimens and the modulus of rupture (f_r) results of the prism (100*100*600) mm, together with the beams according to ASTM [14, 15, 16]. For each series of beams, three specimens were tested, and average values of ($f_c^`$, f_{sp}, and f_r) at 28 days of curing time were found.

8. Experimental Results and Discussions

8.1 Water reduction

Polymers are used to modify the properties of concrete to enhance them more appropriate to work by hand or for other determinations such as saving mechanical energy [18]. Based on the flow test the experimental results in Fig. 3 shows the effect of powder polymer on water-reducing percent.

8.2 Relation between compressive strength and slump test

The slump test is a test to measure the workability of fresh concrete before it sets [17]. Generally, the strength of concrete decreases with an increase in a slump. The increase in slump indicates an increase in the water-cement ratio of concrete. Thus, increasing the w/c ratio causes a decrease in the compressive strength, but Based on experimental data of slump test and compressive test of standard cylinder (150x300) mm of 28 days of curing time, adding polymer to concrete, it was observed that increase in both slump and strength of concrete was parallel together, see Fig. 4.

8.3 Testing of Control Specimens (Cylinders and Prisms)

The compressive strength ($f_c^`$) results of (150x300) mm concrete cylinders indicated that an average increase in the compressive strength of about 39% and 16% were obtained when powder and liquid polymers added respectively, while the addition of polymers resulted in an average increase of about 40% and 16% in the splitting tensile strength (f_{sp}) for the powder and liquid polymer contents respectively. The modulus of rupture (f_r) results of the prism (100*100*600) mm also indicates that the presence of polymer resulted in an increase of about 64% and 59% in the modulus of rupture for the powder and liquid polymer contents respectively. Table 6 summarizes the results of the control specimens.

8.4 Shear failure of beam

Fig. 5 and Table 7 are characterizing the shear failure of beams with and without stirrups along

with the first cracking load, ultimate shear failure load, and type of failure, as measured during testing. In this experimental study, the diagonal cracking load defined as the shear load at the time when the critical diagonal crack (the one that causes failure) is formed within the shear span crossing mid-depth of the beam. It can be distinguished that the values of the diagonal cracking load obtained by using this definition are accurate, such as the ultimate shear failure load.

8.5 Load-Deflection Relation

The load-deflection curves are plotted in groups having beams differing in the parameter (stirrups, types, and content of polymer) considered with the other variables being kept constants as shown in Figs. (6), (7) and (8). Deflections for all beams measured by using an LVDT located at the bottom of mid-span. All load-deflection curves terminated at the points of ultimate loads.

In summary, it can be observed that the presence stirrups and polymer content factors has a greater effect on mid span deflection of the tested beams rather than other factors, the amount of longitudinal bending reinforcement which was kept constant for all beams plays a vital role on deflection of the beams for different values of compressive strengths.

8.6 Shear Crack Width

For measuring the shear crack width of the beam specimens, (LVDT)s were fixed on the right and left sides of each tested beam at the mid-height of its depth, see Fig. 2. Through the (LVDT)s readings, shear crack width of the concrete beams was measured progressively with the load increments. To illustrating the effects of existing of stirrups and different types of polymer on shear crack width, load versus shear crack width diagrams are considering these variables for each beam with and without stirrups as shown in Fig. 9 and Fig. 10, respectively.

It can be observed that for specific stirrups and different types of polymer, existing of stirrups enhanced high strength concrete beams to decrease the shear crack width. On the other hand, for a specific value of polymer content, beams with powder polymer exhibited few shear crack width and far from brittle behavior accompanied by brisker failure. Relationship between measured and predicted values of compressive strength

There is a correlation between the compressive strength ($f_c`$), water to cement ratio (w/c) and of percent of polymer up to 28 days of curing time (t), and $f_c`$ can be found using the following non-linear equation [18].

For HSC:

$$f_c` = 9.27(t)^{0.2}/(w/c)^{0.9} + 0.135(t)^{0.21} * P^{0.16}/(w/c)^{0.75} \quad (1)$$

(R^2= 0.88, Number of data = 75)

Where:

w/c: water to cement ratio in (%), t: curing time in (day)

Admixture: Fly Ash (FA), Silica Fume (SF) and Polymer (P) in (%)

10. Design Equations

10.1 . ACI 318M-14 Equation for Shear Prediction [13]

For members subjected to shear and flexure only, ACI 318M-14 [13] proposed the following equation for predicting the shear strength of reinforced concrete beams. The ACI code has the following equation for calculating the shear force at the section considered (Vu) and nominal shear strength (Vn):

$M_n = As * f_y (d-a/2)$ (fy = 481MPa) (with stirrups)

$a = As * f_y / (0.85 * f_c` * b)$

$\emptyset M_n = M_u$ ($\emptyset$ = 0.9)

$M_u = PL/4 = P = 4 M_u/L$, (effective length L = 100cm)

$V_u = P/2$

$V_c = [0.16 \sqrt{fc`} + 17 \rho (V_u d / M_u)] b_w d \leq 0.29 \sqrt{fc`} b_w d$ (without stirrups)

Table 8 presents the predicted results on the bases of ACI-code and comparison between predicted and test results. The comparison is further presented graphically in Fig. 11.

10.2 . Modified Zsutty's Equation for shear prediction [19]

The following modified Zsutty's equation for predicting the shear capacity of high-strength reinforced concrete beams can be used:

$V_c = 2.1 (f_c' \rho d/a)^{0.33} b_w d$ for $a/d > 2.5$

$V_c = (2.5 [d/a]) * 2.1 (f_c' \rho [d/a])^{0.33} b_w d$ for $a/d \leq 2.5$

Table 9 presents the predicted results. Moreover, the comparison between predicted and test results. The test results are further presented graphically in Fig. 12.

10.3 Proposed Empirical Expressions

Based on analytical work for the 14 tested beams, a proposed equation is reached as below.

$$V_c = 0.1072 [((f_c')^{2.1} (6.02*10^{-9})/ (f_{sp}^{6.7}) + f_{sp}^{1.88}/ 1.93)^{4.25}] b_w d \quad (2)$$

(R^2= 0.88, RMSE= 9.8 MPa)

Comparisons with data of experimental results indicate that the proposed expressions properly estimate the effects of primary factors, such as concrete compressive strength, longitudinal steel ratio, tensile strength, shear span to effective depth ratio. Table 10 and Fig. 13 presents the predicted results of the tested beams according to equation (2) and comparison between predicted and test results.

11. Conclusions

Based on the results and the theoretical analysis of the fourteen tested beams and several Specimens between cylinder and prism of this experimental study on compressive strength, shear strength and behavior of high strength reinforced concrete beams with and without stirrups, using concrete containing 0–1% different types of polymer (powder and liquid) that affected the plastic and hardened properties of concrete, the following conclusions can be drawn:

1- Practically, the compressive strength and workability of concrete modified with different types of polymer (up to 1%) were much higher than the compressive strength and workability of control concrete.
2- Based on experimental work, the optimum quantity of powder polymer (F and B) content of dry weight of cement for HSC was 0.20% for workability and mechanical properties.
3- The growth of compressive strength of concrete modified with polymer was increased by 35-38% at 28th days of curing time, when 0.2% of the powder polymer was added to the concrete compared with control concrete.
4- The splitting tensile strength of concrete modified with different types of the polymer was increased by 38-40%, the flexural strength 61-65%.
5- Based on the experimental results of mechanical properties of concrete modified with powder and liquid polymers observed that the powder F and B have higher effects than liquid L2 and L4 by 2-4%.
6- Using stirrups as web reinforcement has a significant effect on shear strength of tested specimens, for concrete by 42% and for concrete modified with polymer 69%.
7- High strength concrete beams without stirrups showed a brittle behavior than with stirrups, and the experimental results support that the effect of the addition of stirrups has reduced the brittle failure of the beams, by 58%.
8- In general, with increasing compressive strength, the failure loads and consequently the shear strength of the tested beams increased significantly, because enhancing of polymer's effects.

References

1- Schmidt, W. "Design concepts for the robustness improvement of self-compacting concrete". Eindhoven University of Technology, the Netherlands. Doctor of Philosophy. Vol. 30 (9), (2014), pp. (130-159).
2- Aïtcin, P. C. "Cements of yesterday and today: concrete of tomorrow". Cement and Concrete research, Vol. 30 (9), (2000), pp. (1349-1359).
3- Sabet, F. A., Libre, N. A., & Shekarchi, M. "Mechanical and durability properties of self-consolidating high performance concrete incorporating natural zeolite, silica fume and fly ash". Construction and Building Materials, Vol. 44 (1), (2013), pp. (175-184).
4- Park, C. K., Noh, M. H., & Park, T. H. "Rheological properties of cementitious materials containing

تاثير استخدام أنواع مختلفة من البوليمرات على مقاومة القص لعتبات بسيطة الاسناد من الخرسانة المسلحة عالية المقاومة

سامان كمال[1] - طالب ماجستير
د . جلال احمد سعيد[1] - استاذ
[1]جامعة السليمانية ، كلية الهندسة ، قسم الهندسة المدنية

المستخلص

هذا العمل هو محاولة لدراسة سلوك مقاومة القص للخرسانة المسلحة عالية المقاومة (المعدلة مع أنواع مختلفة من البوليمرات) للعتبات مع وبدون تسليح القص. تم اختبار 14 عتبة من الخرسانة المسلحة بسيطة الاسناد تحت حمل مركزي في مجموعتين (مع وبدون تسليح القص). جميع الحزم لها نفس المقطع 300*200 ملم ، بطول 1200 ملم مع نفس التسليح. المتغيرات الرئيسية التي تمت دراستها هي مقاومة الانضغاط، تعزيز القص ، وانواغ والنسب المئوية من البوليمرات.

تعزيز الخواص الميكانيكية للخرسانة بإضافة أنواع مختلفة من البوليمر (باودر وسائل) تصل إلى1% ، تسببت في انخفاض نسبة الماء إلى الأسمنت من 0.35 إلى 0.23. النمو في مقاومة الانضغاط39% ، زيادة مقاومة الانفلاق 40% ، تحسين مقاومة الانثناء65%. بينما ، في حين أستعمال البوليمر السائل ، نمو قوة الانضغاط بنسبة 14% ، زيادة قوة مقاومة الانفلاق16% ، تحسين قوة الانثناء 59%. من هذه النتائج و استنادا الى التحليل الاحصائي ، تم رسم نموذج رياضي للخرسانة عالية المقاومة المعدلة بالموليمرات

الكلمات المفتاحية : العتبات ، مقاومة الانضغاط ، كونكريت عالي المقاومة ، مقاومة القص ، بولمير ، تسليح القص

mineral admixtures". Cement and concrete research, Vol. 35 (5), (2005), pp. (842-849).
5- Ghosh, S. K. "High strength concrete in US codes and standards". In XIV Congreso Nacional de Ingeniería Estructural. Vol. 97 (4), July-August, 2004, pp. (1-16).
6- ACI Committee 363. "Report on High-Strength Concrete (ACI 363R-10)". ACI materials journal, Vol.7 (2), (2010), pp. (1-65).
7- Logan, A., Choi, W., Mirmiran, A., Rizkalla, S., & Zia, P. "Short-term mechanical properties of high-strength concrete". ACI materials journal, Vol. 106 (5), (2009), pp. (413).
8- Moslev, W. H., Hulse, R., & Bungev, J. H. "Reinforced concrete design: to Eurocode 2". Macmillan International Higher Education. 7th ed. 2012 edition (April 10, 2012), pp. (1-464).
9- Kim, J. K., & Park, Y. D. "Prediction of shear strength of reinforced concrete beams without web reinforcement". American Concrete Institute. ACI Materials Journal, Vol. 93 (M24), (1996), pp. (213-222).
10- ASTM, C150-17, "Standard Specification for Portland Cement". West Conshohocken, PA. Annual book of ASTM standards, Vol. 5 (1), (2017), pp. (13-25).
11- ASTM C33, "Standard specification for concrete aggregates" American Society for Testing and Material, Annual book of ASTM standards, Vol. 4 (2), (2004), pp. (1-11).
12- ASTM, A615/A615M-09b, "Standard specification for deformed and plain carbon-steel bars for concrete reinforcement". Annual book of ASTM standards, Vol. 3(4), (2009), pp. (325-339).
13- American Concrete Institute (ACI), "(ACI 318-14), Building Code Requirements for Structural Concrete" Concrete International, Vol. 41(8), (2014), pp. (1-492).
14- ASTM, C39/ 39M-05. Standard test method for compressive strength of cylindrical concrete specimens, ASTM International, West Conshohocken, PA. Vol. 4(2), (2005), pp. (115-125).
15- ASTM, C496/C496M-04. "Standard Test Method for Splitting Tensile Strength of Cylindrical Concrete Specimens. Vol. 4(1), (2004), pp. (101-113).
16- ASTM, C 78-10. Standard test method for flexural strength of concrete (using simple beam with third-point loading). In American society for testing and materials Vol. 100 (2), (2010), pp. (128-159).
17- ASTM, C494/C494M-13. "Standard specification for chemical admixtures for concrete". Annual book of ASTM standards. Annual book of ASTM standards, Vol. 4 (1), (2013), pp (256-263).
18- Saman M. K., University of Sulaimani, (2019). "Effect of using polymers on shear strength of high strength reinforced concrete beams", MSc. Thesis, pp. (79-87).
19- Faisal F. Wafa, Samir A. Ashour and Ghazi S. Hasanain, " Shear Behavior of Reinforced High-Strength Concrete Beams Without Shear Reinforcement", Engineering Journal of Qatar University, Vol. 7 (1), (1994), pp. (91-113).

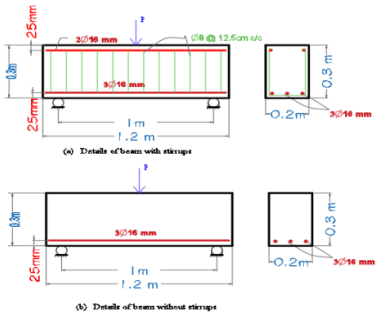

Fig. 1: Details of the beam specimens, (a) with stirrups, and (b) without stirrups.
(Source: Researcher)

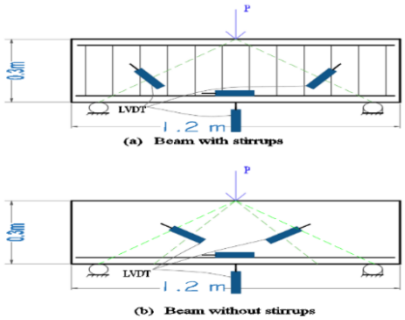

Fig. 2: Location of the LVDTs, (a) with stirrups, and (b) without stirrups.
(Source: Researcher)

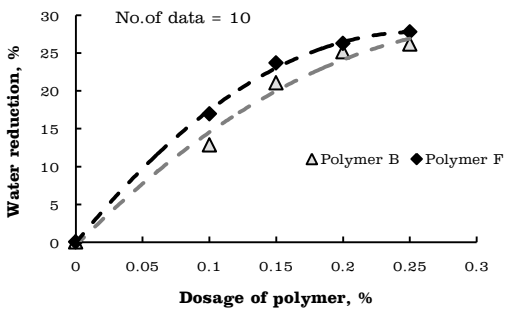

Fig. 3: Effect of two types of powder polymers on water reduction percent (experimental data). (Source: Researcher)

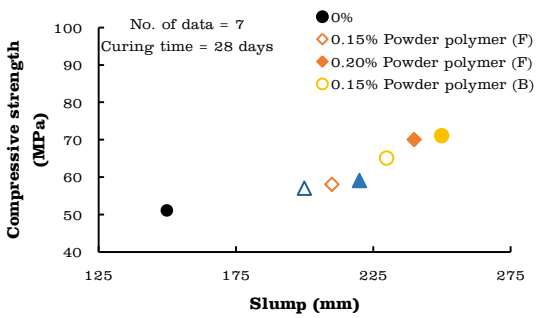

Fig. 4: The relation between compressive strengthand slump test (experimental data).
(Source: Researcher)

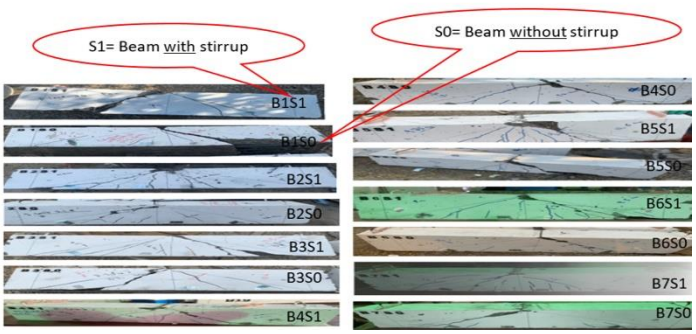

Fig. 5: Crack patterns for beams. (Source: Researcher)

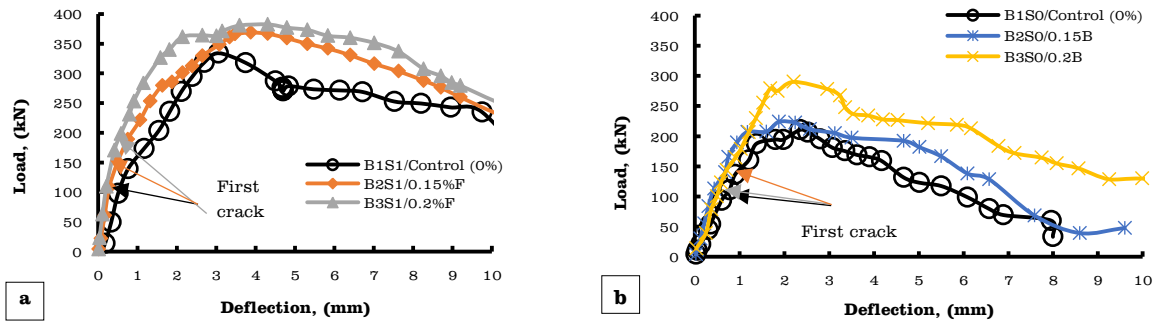

Fig. 6: Load- Deflection Curves of reinforced concrete beams modifiedwith polymer (F) Beams (a)with and (b)without stirrups. (Source: Researcher)

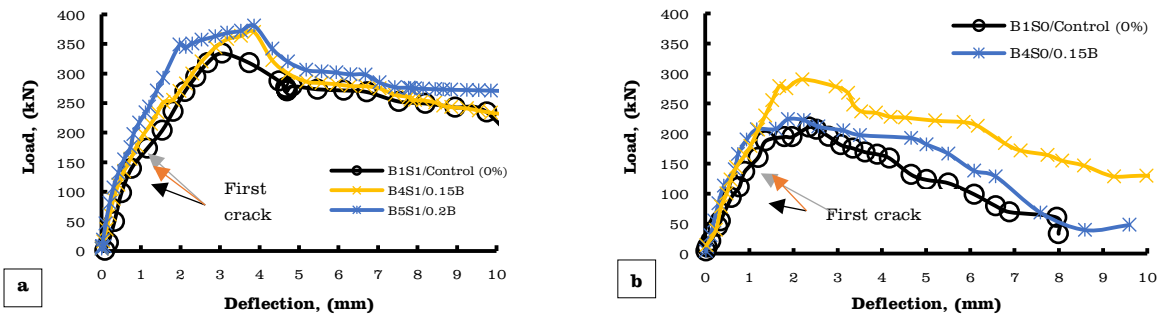

Fig. 7: Load- Deflection Curves of reinforced concrete beams modified with polymer (B) Beams (a)with and (b)without stirrups. (Source: Researcher)

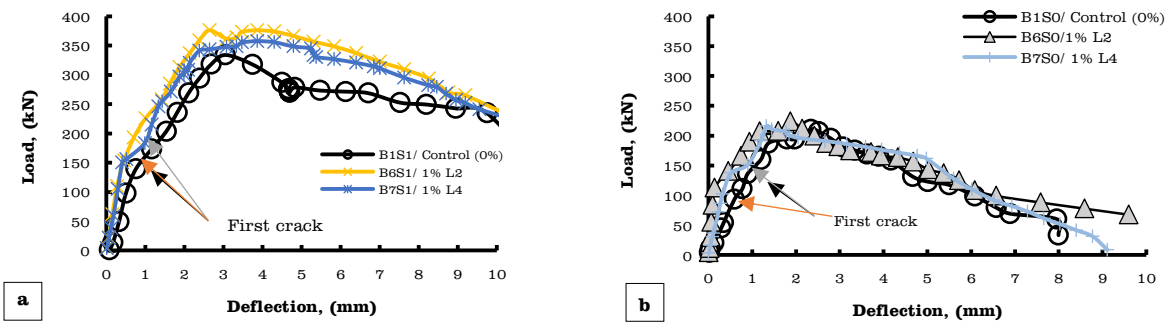

Fig. 8: Load- Deflection Curves of reinforced concrete beams modifiedwith polymer (L2 and L4) Beams (a)with and (b)without stirrups. (Source: Researcher)

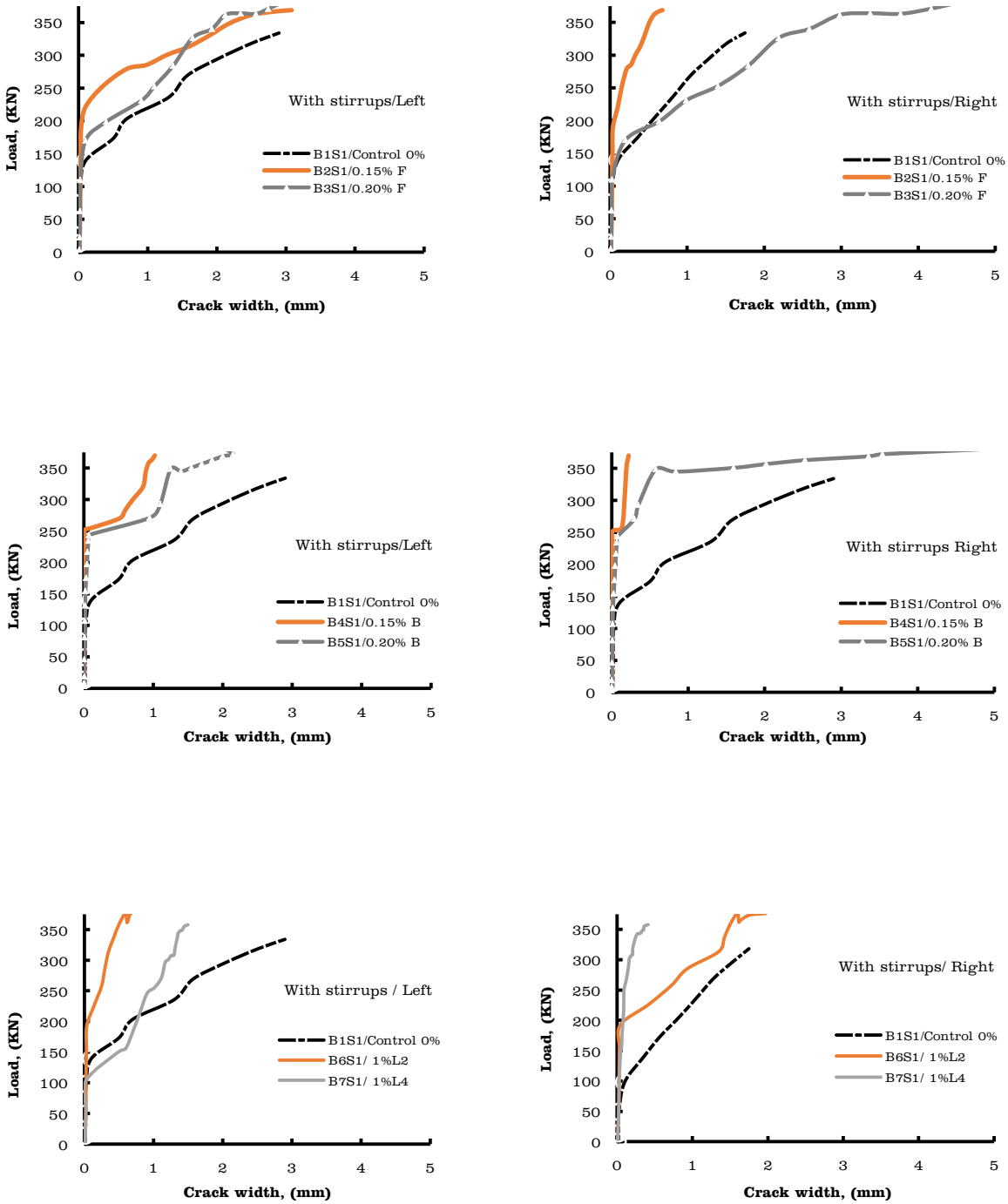

Fig. 9: The relation between load and shear crack width of beams with stirrups. (Source: Researcher)

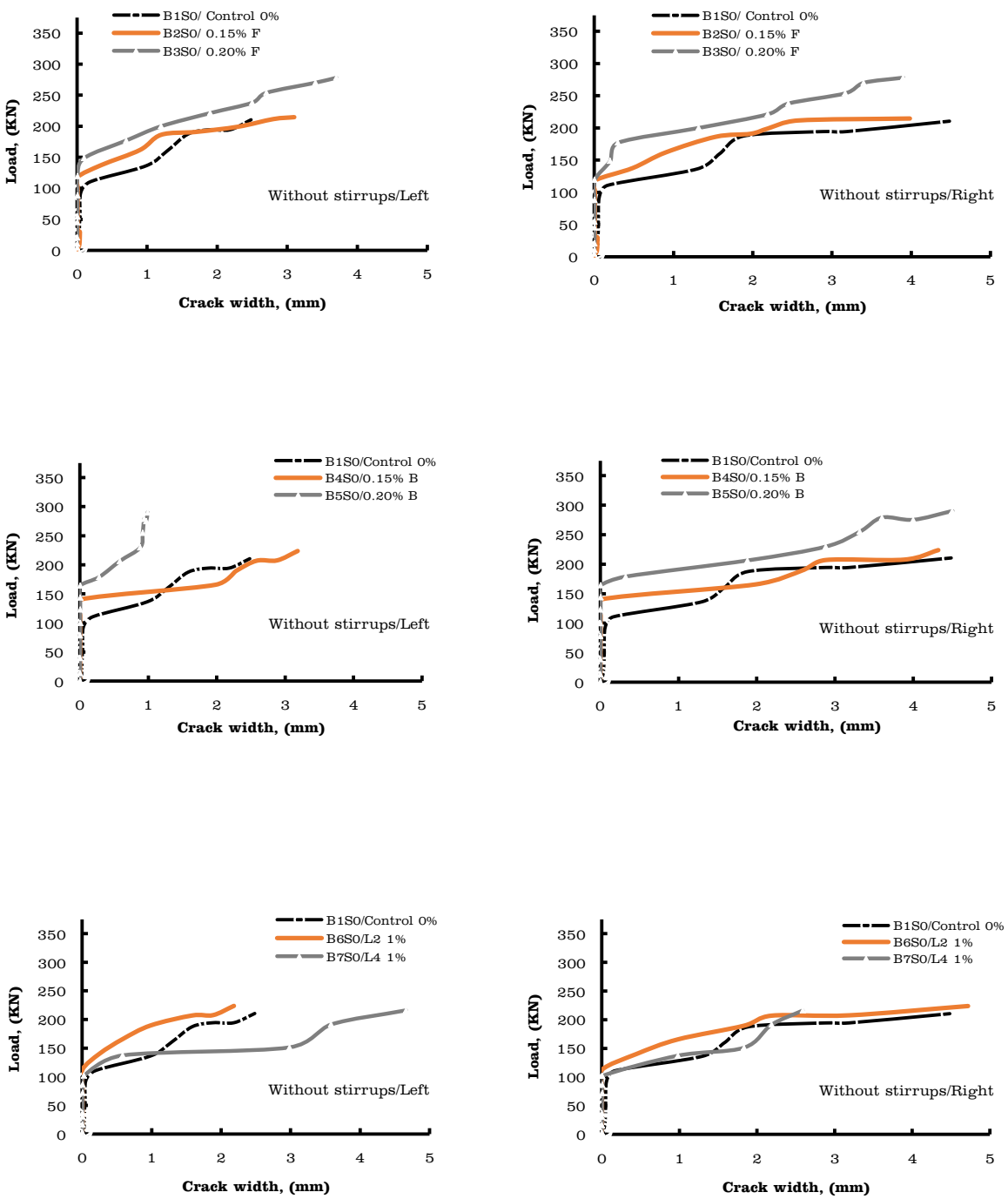

Fig. 10: The relation between load and shear crack width of beams without stirrups. (Source: Researcher)

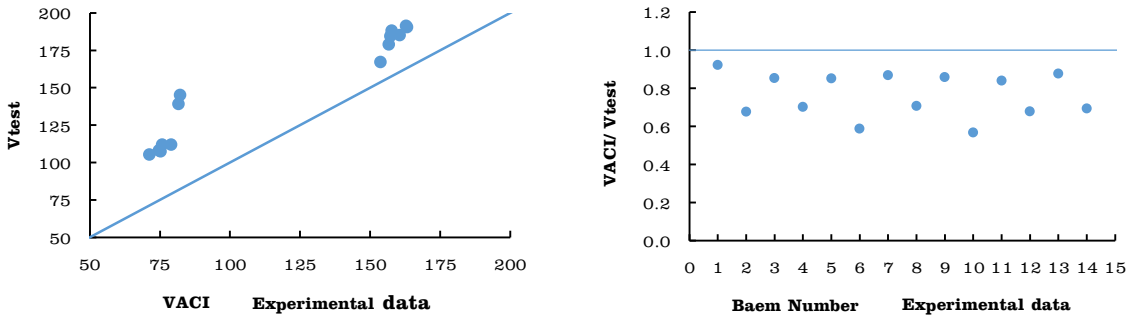

Fig. 11: Comparison of the Test and the Predicted Results Based on the ACI 318M-14 [13] Equation. (Source: Researcher)

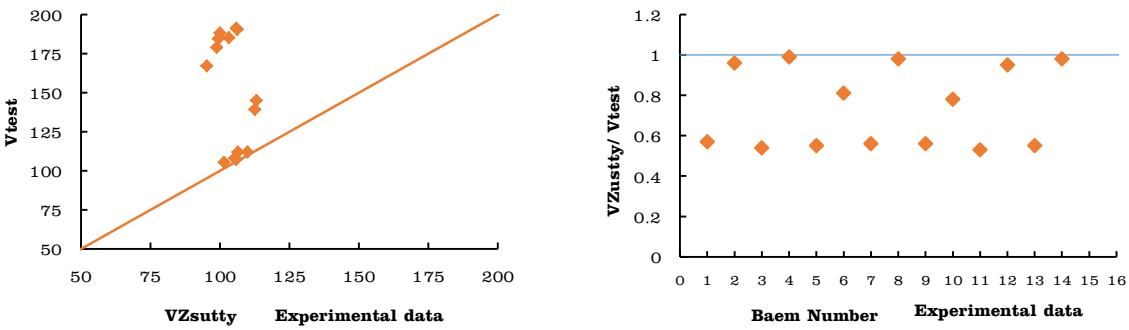

Fig. 12: Comparison of the Test and the Predicted Results Based on the Zsutty's Equation. (Source: Researcher)

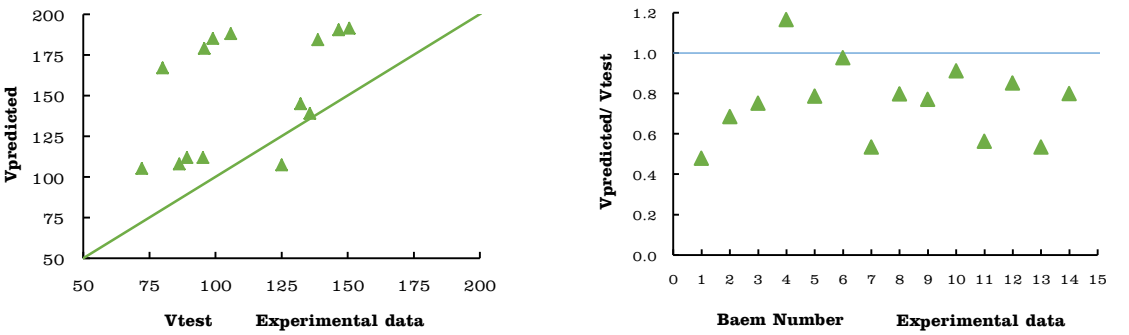

Fig. 13: Comparison of the Test and the Predicted results according to Eq. (2). (Source: Researcher)

Table 1: Classifications and Details. (Source: Researcher)

Series	Beam	Polymer content	Series	Beam	Polymer content
1	B1S1* B1S0**	0%	5	B5S1* B5S0**	F, 0.2%
2	B2S1* B2S0**	B, 0.15%	6	B6S1* B6S0**	L2, 1%
3	B3S1* B3S0**	B, 0.2%	7	B7S1* B7S0**	L4, 1%
4	B4S1* B4S0**	F, 0.15%	*S1: With stirrups **S0: Without stirrups		

Table 2: Physical properties of cement. (Source: Researcher)

Physical properties	Results	ASTM C150 [10] Specification
Consistency	24.9%	
Compressive strength For 3 days For 7 days	32.3MPa 39.0 MPa	Lower limit 12 MPa Lower limit 19 MPa
Setting Time Initial setting time Final setting time	 155 minutes 202 minutes	 Not less than 45 minutes Not more than 600 minutes

Table 3: Chemical composition of Gasin Cement. (Source: Researcher)

Chemical test	Results (%)	ASTM C150 [10] Specification
SiO_2 (Silica)	19.90	....
CaO (Lime)	63.33	....
Al_2O_3 (Alumna)	4.09	....
Fe2O3 (Iron oxide)	4.91	....
MgO (magnesia)	1.80	5.0% max.
SO_3 (Sulfate)	2.24	2.8% max.
C_3A (Tri calcium aluminate)	2.55	....
L.S.F (Lime saturation factor)	0.98	(0.66-1.02)
C_3S (Tri calcium silicate)	67.89	....
C_2S (Dia calcium silicate)	5.05	....
C4AF (Tetra calcium alumina ferrite	14.92	....
L.O.I (Loss of ignition)	3.41	4.0% max.
Insoluble material	0.49	1.5% max.

Table 4: The properties of powder polymers used. (Source: Researcher)

Designation		B	F
Commercial name		DBC-21	VX-98
Solid content (%)		>97	>97
PH value		6-8	9-11
Water reduction (%)		> 25	> 25
Air content (%)		≤ 3	≤ 3
Setting time (%)	Initial	>+ 40	>+ 40
	Final	>+ 30	>+ 40
Compressive strength (%)	1day	210	210
	3days	190	190
	7days	180	180
	28days	170	170
Chloridion (%)		< 0.1	< 0.1
Alkali (%)		< 5	< 5

Table 5: The properties of liquid polymers used. (Source: Researcher)

Designation	L2	L4
Commercial Name	SP633T	SIF N PUL
Appearance	Light Brown Liquid	Dark Brown Liquid
Density (Kg/m^3)	1.03-1.09	1.11-1.17
PH Value	7.0-10.0	7.0-11.0
Dosage by weight of cement	0.2-2.5%	0.6-2.0%
Approval/ Standard	EN 934-2+A1:2012:T3	ASTM C494-86 Type A&F

Table 6: Average test results of cylinder specimens (150*300) mm and prism (100*100*600) mm at 28 days of curing time. (Source: Researcher)

Series	Polymer content	Compressive strength, $f_c`$ (MPa)	% increase in $f_c`$	Tensile strength, f_{sp} (MPa)	% increase in f_{sp}	Modulus of rupture, f_r (MPa)	% increase in f_{sp}
1	0%	51	0	5	0	7.5	0
2	F, 0.15%	58	14	5.6	12	11.1	48
3	F, 0.2%	70	37	6.9	38	12	60
4	B, 0.15%	65	27	6.7	34	11.4	52
5	B, 0.2%	71	39	7	40	12.3	64
6	L2, 1%	59	16	5.8	16	11.9	59
7	L4, 1%	57	12	5.5	10	11.6	55

Table 7: Summary of Results of the Tested Beams. (Source: Researcher)

Series	Beam	f_c` (MPa)	Polymer content	ρ_w *	b_w mm)	d (mm)	First shear crack load (kN)	Failure load (kN)	Mode of failure
1	B1S1	51	0%	0.0116		259	139.3	334	
	B1S0			0.0113		267	110.9	210.5	
2	B2S1	58	F, 0.15%	0.0116	200	259	150.8	368.8	
	B2S0			0.0113		267	137.6	214.6	
3	B3S1	70	F, 0.2%	0.0116	200	259	170.4	382.5	
	B3S0			0.0113		267	148.6	278.1	
4	B4S1	65	B, 0.15%	0.0116	200	259	255.4	370	
	B4S0			0.0113		267	165.6	223.7	
5	B5S1	71	B, 0.2%	0.0116	200	259	271.1	380.7	
	B5S0			0.0113		267	179	290	
6	B6S1	59	L2, 1%	0.0116	200	259	225.7	376.1	
	B6S0			0.0113		267	140.3	223.7	
7	B7S1	57	L4, 1%	0.0116	200	259	150.4	357.7	
	B7S0			0.0113		267	137.2	215.9	

Shear failure

*: ρ = Longitudinal tensile reinforcement ratio=A_f/ (b_w d)

Table 8: Test and Predicted Shear Results Based on ACI 318M-14 Equation. (Source: Researcher)

Series	Beam	f_c' (MPa)	Polymer content	ρ	d (mm)	Vc_{ACI} (kN)	Vn_{ACI} (kN)	V_{test} (kN)	V_{ACI}/ V_{test}
1	B1S1*	51	0%	0.0116	259		154	167	0.92
	B1S0**			0.0113	267	71		105	0.68
2	B2S1*	58	F, 0.15%	0.0116	259		157	184	0.85
	B2S0**			0.0113	267	75		107	0.70
3	B3S1*	70	F, 0.2%	0.0116	259		163	191	0.85
	B3S0**			0.0113	267	82		139	0.59
4	B4S1*	65	B, 0.15%	0.0116	259		161	185	0.87
	B4S0**			0.0113	267	79		112	0.71
5	B5S1*	71	B, 0.2%	0.0116	259		163	190	0.86
	B5S0**			0.0113	267	82		145	0.57
6	B6S1*	59	L2, 1%	0.0116	259		158	188	0.84
	B6S0**			0.0113	267	76		112	0.68
7	B7S1*	57	L4, 1%	0.0116	259		157	179	0.88
	B7S0**			0.0113	267	75		108	0.69
							Mean	0.76	
							Standard deviation	0.116	
							Coefficient of variance	15.21	

Table 9: Test and Predicted Shear Results Based on Modified Zsutty's Equation. (Source: Researcher)

Series	Beam	$f_c`$ (MPa)	Polymer content	ρ	a/d	d (mm)	V_{Zsutty} (kN)	V_{test} (kN)	V_{Zsutty}/V_{test}
1	B1S1	51	0%	0.0116	1.87	259	95	167	0.57
	B1S0			0.0113	1.93	267	102	105	0.96
2	B2S1	58	F, 0.15%	0.0116	1.87	259	100	184	0.54
	B2S0			0.0113	1.93	267	106	107	0.99
3	B3S1	70	F, 0.2%	0.0116	1.87	259	106	191	0.55
	B3S0			0.0113	1.93	267	113	139	0.81
4	B4S1	65	B, 0.15%	0.0116	1.87	259	103	185	0.56
	B4S0			0.0113	1.93	267	110	112	0.98
5	B5S1	71	B, 0.2%	0.0116	1.87	259	106	190	0.56
	B5S0			0.0113	1.93	267	113	145	0.78
6	B6S1	59	L2, 1%	0.0116	1.87	259	100	188	0.53
	B6S0			0.0113	1.93	267	107	112	0.95
7	B7S1	57	L4, 1%	0.0116	1.87	259	99	179	0.55
	B7S0			0.0113	1.93	267	105	108	0.98
						Mean			0.74
						Standard deviation			0.2008
						Coefficient of variance			27.25

Table 10: Test and Predicted shear results according to Eq. (2). (Source: Researcher)

series	Beam	$f_c`$ (MPa)	f_{sp} (MPa)	Polymer content	ρ	a/d	d (mm)	$V_{predicted}$ (kN)	V_{test} (kN)	$V_{Predicted}$ / V_{test}
1	B1S1	51	5	0%	0.0116	1.87	259	80	167	0.41
	B1S0				0.0113	1.93	267	72	105	0.25
2	B2S1	58	6.7	F, 0.15%	0.0116	1.87	259	139	184	0.41
	B2S0				0.0113	1.93	267	125	107	0.52
3	B3S1	70	7	F, 0.2%	0.0116	1.87	259	151	191	0.56
	B3S0				0.0113	1.93	267	136	139	0.78
4	B4S1	65	5.6	B, 0.15%	0.0116	1.87	259	99.	185	0.38
	B4S0				0.0113	1.93	267	89.	112	0.46
5	B5S1	71	6.9	B, 0.2%	0.0116	1.87	259	147	190	0.50
	B5S0				0.0113	1.93	267	132	145	0.39
6	B6S1	59	5.8	L2	0.0116	1.87	259	106	188	0.27
	B6S0				0.0113	1.93	267	95	112	0.35
7	B7S1	57	5.5	L4	0.0116	1.87	259	96	179	0.55
	B7S0				0.0113	1.93	267	86	108	0.33
							Mean		0.76	
							Standard deviation		0.190	
							Coefficient of variance		25.08	